HAZARD ASSESSMENT AND INUNDATION MODELING OF PALAU, REPUBLIC OF PALAU

Natalia Sannikova
Christopher Moore

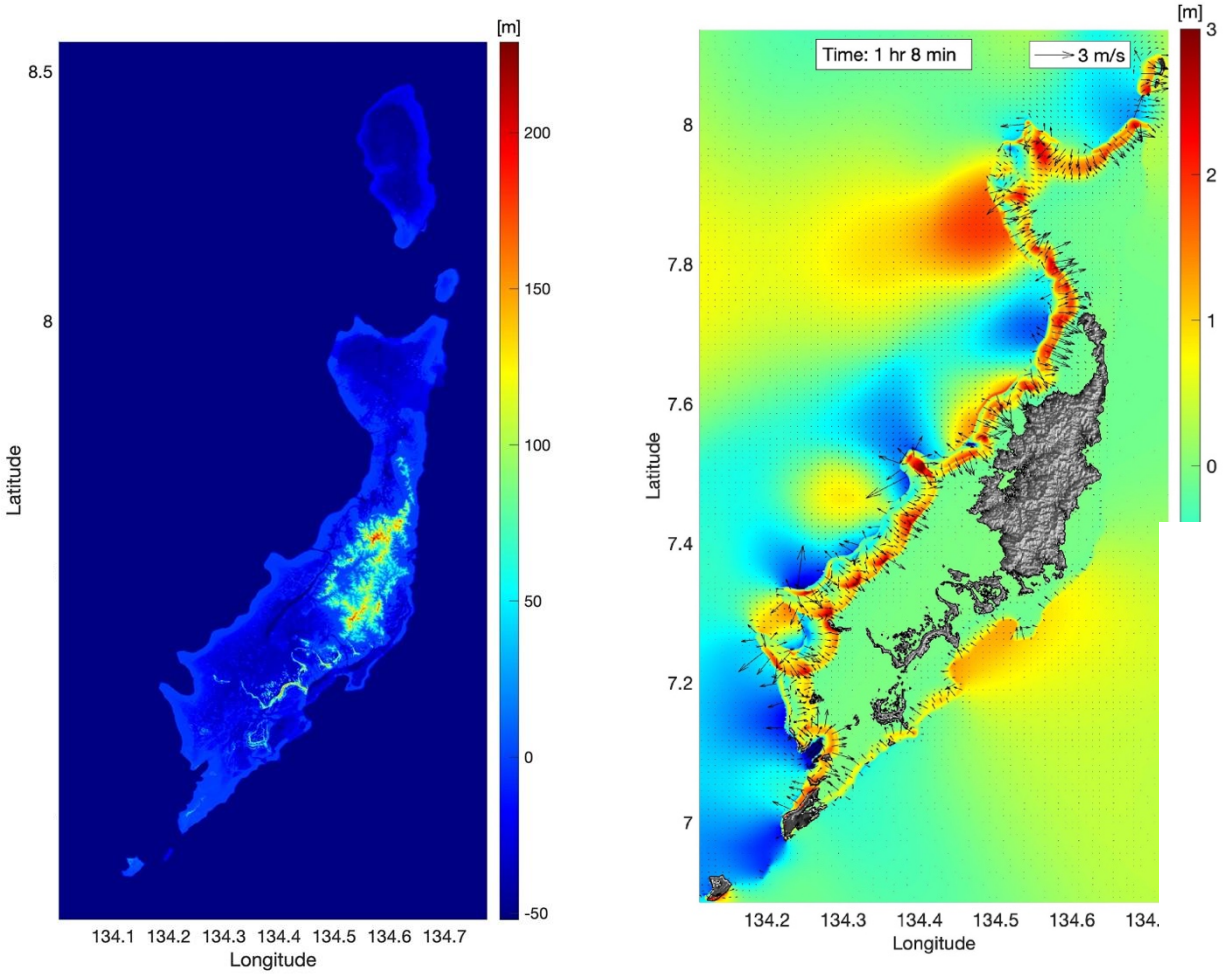

NOAA CENTER FOR TSUNAMI RESEARCH
PACIFIC MARINE AND ENVIRONMENTAL LABORATORY
SEATTLE, WA
September 2024

NOTICE from NOAA

Mention of a commercial company or product does not constitute an endorsement by the United States National Oceanic and Atmospheric Administration Office of Atmospheric Research (NOAA/OAR). Use of information from this publication concerning proprietary products or the tests of such products for publicity or advertising purposes is not authorized. Any opinions, findings, and conclusions or recommendations expressed in this material are those of the authors and do not necessarily reflect the views of the National Oceanic and Atmospheric Administration.

HAZARD ASSESSMENT AND INUNDATION MODELING OF PALAU, REPUBLIC OF PALAU

Natalia Sannikova[1,2]
Christopher Moore[1]

[1] NOAA/Pacific Marine Environmental Laboratory (PMEL), Seattle, WA
[2] *Cooperative Institute* for Marine and Atmospheric Research, Honolulu, HI

September 2024

Acknowledgements

The authors wish to thank Dr. Laura Kong and Tammy Fukuji of the International Tsunami Information Center for project direction and assistance with the acquisition of bathymetry and topography data. The authors also thank Marie Eble for review and editing of this report. LIDAR and near-shore data were shared with NOAA by the Government of Palau and the Coral Reef Research Foundation (CRRF) to support tsunami hazard assessment and inundation modeling for Palau. Funding for this work was provided by the United States Agency for International Development Bureau of Humanitarian Affairs (USAID/BHA) to the U.S. NOAA International Tsunami Information Center for implementing the UNESCO-IOC Tsunami Ready Recognition Programme in Palau. The tsunami goal of the United Nations Decade of Ocean Science for Sustainable Development 2021-2030 is to make 100% of communities at risk from tsunamis prepared and resilient to tsunamis by 2030 through Tsunami Ready and other similar initiatives.

Abstract

An earthquake scenario-based tsunami hazard assessment was conducted for the Republic of Palau. Historical events guided a sensitivity study that was conducted to identify specific source regions with the greatest potential to generate tsunamis most hazardous to Palau. The NOAA Tsunami Forecast Propagation Database was used to model tsunami impact along the coastline of Palau from tsunami originating from 138 discrete earthquake sources. Study results identified two sources originating from the East Philippine Subduction Zone and two sources along the Yap-Palau Trenches as posing the greatest risk to Palau. Tsunami waves from these four potentially most hazardous sources were then numerically generated to determine the impact on Palau of tsunami using the high-resolution Digital Elevation Model (DEM) and calculation grid. The non-linear shallow water wave inundation model Hyperbolic Systems and Efficient Algorithms (HySEA) was used to determine travel, arrival and duration times, maximum wave amplitudes, tsunami heights, flow depths, inundation, current speeds and attenuations. The time series that were generated for specific locations provide a well-documented reference and basis for tsunami evacuation mapping and planning by Palau agencies responsible for the safety of residents and visitors to the islands.

1. Introduction

This report documents the tsunami inundation modeling for Palau performed by the tsunami research group at the NOAA Pacific Marine Environmental Lab (PMEL) in Seattle, WA. The results of the modeling study produced inundation data for the purpose of developing evacuation maps and procedures for Palau under the UNESCO IOC Tsunami Ready Recognition Programme being supported by the International Tsunami Information Center. Advances in tsunami modeling and hardware make it possible to model Palau tsunami inundation at high resolution (10 m). The Republic of Palau is surrounded by the Pacific Ocean “Ring of Fire” – extremely active seismic zones, which align with the boundaries of the tectonic plates. The historic record of the region also confirms past tsunamis affecting the region. The subduction zones (SZ) of the Pacific Ocean that are identified as tsunamigenic were considered, and sources with significant impact to Palau were included in the study. The largest credible seismic

scenarios that impinge on Palau were identified and modeled with a fully nonlinear shallow water wave model from initial deformation to regional propagation to inundation. Hazards from inundation and currents were assessed for each source, and composite maximum plots were created which are suitable for creating evacuation maps and plans.

2. Study Area

Palau is the westernmost archipelago in the chain formerly known as the Caroline Islands, which includes Yap, Chuuk, Pohnpei, and Kosrae (the Federated States of Micronesia). All but six of Palau's islands are located close by and form the main Palau group (Figure 1). The total area consists of 340 islands and is 466 square kilometers. Its most populous islands are Angaur, Babeldaob, Koror and Peleliu. The latter three lie together within the same barrier reef, while Angaur is an oceanic island several kilometers to the south. About two-thirds of the population lives on Koror (Figure 2). The coral atoll of Kayangel is north of these islands, while the uninhabited Rock Islands (about 200) are west of the main island group. A remote group of six islands, known as the Southwest Islands, some 604 kilometers (375 miles) from the main islands, make up the states of Hatohobei and Sonsorol.

The study area consists of the Main Palau Group including the fourteen most populated states (out of sixteen) where 99.5% of the population live (Census, 2021). The two remote states require additional research due to its distant location from the main group.

Land and Resource Information System Office, Palau (PALARIS) shared with PMEL the Light Detection and Ranging (LiDAR) Digital Elevation Map (DEM) with very high resolution (1 m) with Palau wide coverage. The US Tsunami Hazard Mitigation Program (NTHMP)-approved and benchmarked HySEA model (NTHMP, 2017) was selected to allow full-island modeling at high resolution, including all critical infrastructure.

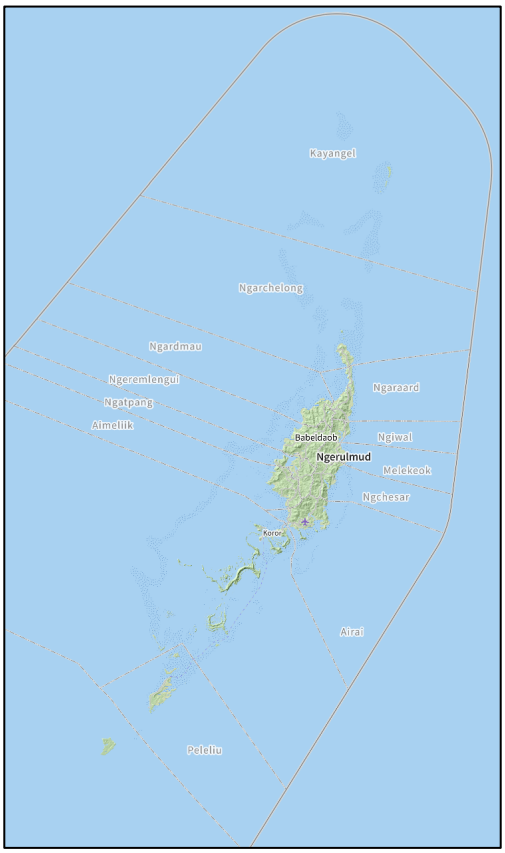

Figure 1. The main Palau group (OpenStreetMap, 2024).

Figure 2. Koror – the largest city and the commercial center in Palau (picture credits to https://www.unusualtraveler.com/).

3. Regional Seismicity and Tsunami Event History

The Republic of Palau is an island country in the Pacific Ocean's "Ring of Fire" – a string of volcanoes and sites of seismic activity, or earthquakes, around the edges of the Pacific Ocean. Roughly 90% of all earthquakes occur along the Ring of Fire, and the ring is dotted with 75% of all active volcanoes on Earth. Following NOAA National Centers for Environmental Information (NCEI) Global Historical Tsunami Database there were 10 different earthquake and earthquake and slide-generated tsunami that ever affected Palau (NCEI, 2024). All of them originated from the Ring of Fire: four from the Philippine, four from New Guinea, one from Japan and one from the Kuril-Kamchatka Trenches (Figure 3). The biggest tsunami runups of 33 cm and 20 cm at Angaur Island were measured from 03/19/1952 Mw 7.3 Mindanao, Philippines Tsunami and 03/04/1952 Mw 8.1 SE Hokkaido Island Tsunami accordingly. 9 of 10 tsunami were measured instrumentally at the tide gauge.

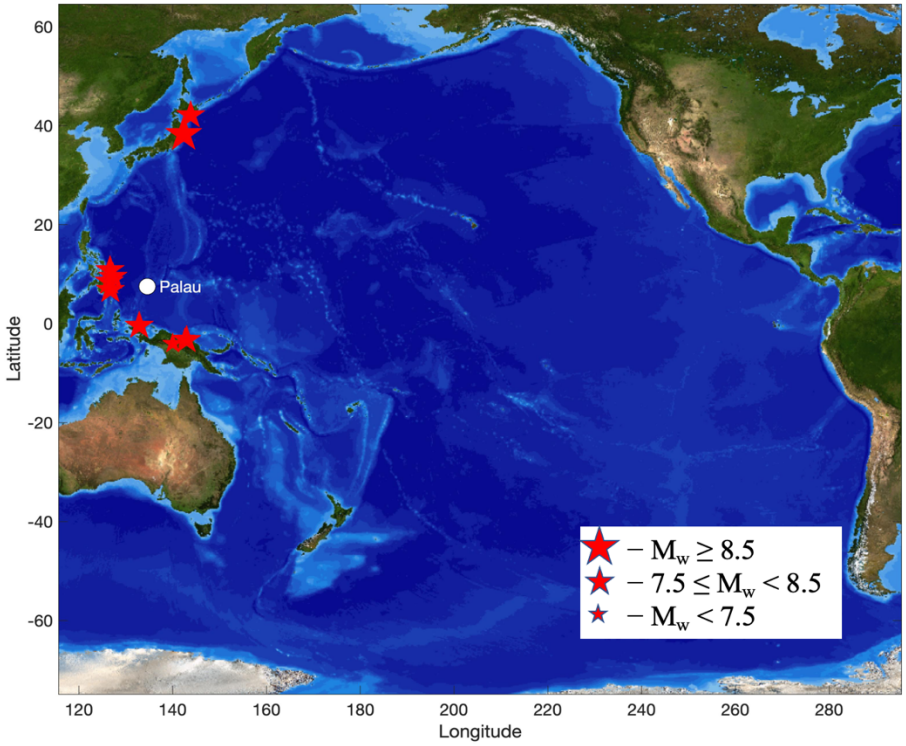

Figure 3. The distribution of the earthquake and earthquake and slide generated tsunami events that ever affected Palau over the Pacific Ocean SZs.

3.1. Regional Seismicity

South Pacific Island Countries are located close to one of the most active SZs in the world and are prone to high seismic risk. Since the year 2000, thirty-nine earthquakes of moment magnitude (*Mw*) greater than or equal to 7.5 have occurred in the region, with seven having *Mw*>8.0 (USGS). The complicated tectonics and the high seismicity of the region are due mainly to the interaction of four major plates (Figure 4), the Pacific, Philippine Sea, Sunda, and Australia plates. The Philippine Sea plate subducts to the west under the Sunda plate at a rate of about 100 mm/year, and the Australia plate subducts to the north beneath the Sunda plate at a rate of about 70 – 80 mm/year. The convergence between the Australia and Pacific plates results in a shortening at the subduction plate boundaries along Papua New Guinea, the Solomon Islands, Vanuatu, Fiji and Tonga. The convergence rate is about 60 – 70 mm/year at the Tonga trench, and about 100 mm/year at other trenches (Rong et al., 2016).

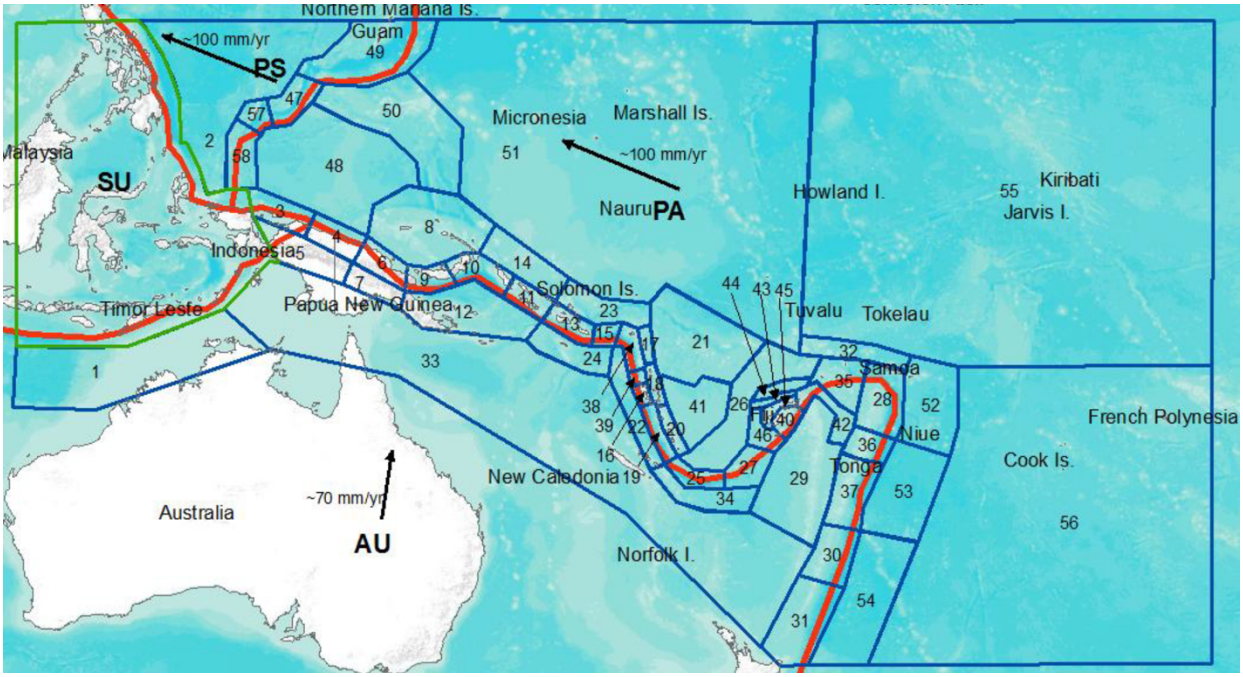

Figure 4. Regional tectonic setting and seismic source zones in the South Pacific region. Thick red lines indicate the major plate boundaries between the four major plates: Pacific (PA), Philippine Sea (PS), Sunda (SU), and Australia (AU) plates. Thick black arrows illustrate the movement of the PA, PS, and AU plates relative to the SU plate (Bird, 2003). The source zones are illustrated by blue polygons, and the numbers are the zone IDs (Rong et al., 2016).

3.2. Tsunami Events

Table 1 contains information about 10 earthquake or earthquake and slide generated tsunami that ever affected Palau (NCEI, 2024). All of them originated from the active SZs: South Pacific (Philippine, New Guinea Trenches) and Kuril-Kamchatka, Japan Trenches (Figure 5).

Table 1: Historical tsunami events that affected Palau (NCEI, 2024).

Date	Date	Source Country	Source Longitude	Source Latitude	M_w	Affected Area	Runup
1	12/2/2023	Philippines, E. Mindanao Island	126.449	8.527	7.6	Malakal Island, Caroline Islands	1 cm
2	8/31/2012	Philippines, Philippine Islands	126.638	10.811	7.6	Malakal Island, Caroline Islands	2 cm
3	3/11/2011	Japan, Honshu Island	142.372	38.297	9.1	Malakal Island, Caroline Islands	16 cm
4	1/3/2009	Indonesia, near North Coast	132.885	-0.414	7.6	Malakal Island, Caroline Islands	4 cm
5	9/8/2002	Papua New Guinea, Bismarck Sea	142.940	-3.260	7.6	Malakal Island, Caroline Islands	
6	7/17/1998	Papua New Guinea	142.582	-2.943	7	Malakal Island, Caroline Islands	2 cm
7	1/10/1970	Philippines, Philippine Trench	126.700	6.8	7.6	Malakal Island, Caroline Islands	6 cm
8	3/19/1952	Philippines, E. of Mindano	127.250	9.5	7.8	Angaur Island	33 cm
9	3/4/1952	Japan, SE. Hokkaido Island	143.850	42.150	8.1	Angaur Island	2 cm
10	10/7/1900	Indonesia, Bismarck Sea	140.000	-4	6.9	Tobi Island	

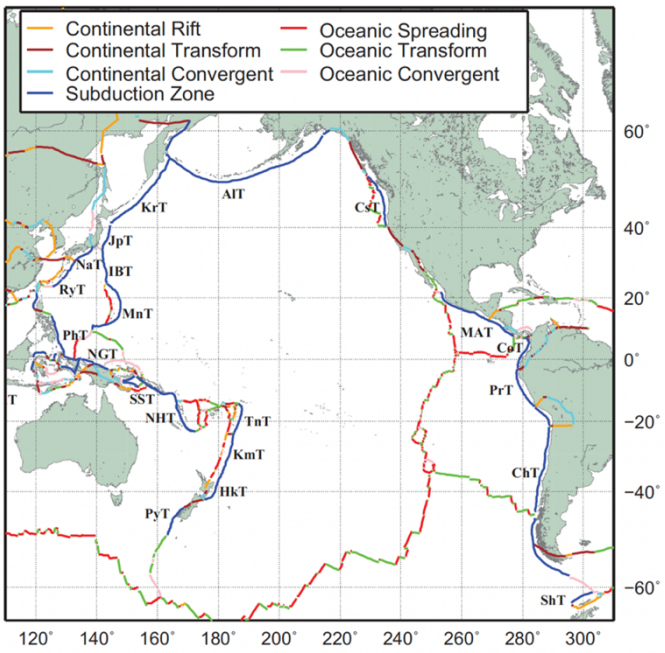

Figure 5. Map of major plate boundaries in the Pacific Ocean with SZs shown (in blue) and labeled as follows: AlT-Aleutian Trench, ChT-Chile Trench, CsT-Cascadia Trough, HT-Hikurangi Trough, IBT-Izu-Bonin Trench, JpT-Japan Trench, KmT-Kermadec Trench, KrT-Kuril Trench, MT-Mariana Trench, MAT-Middle America Trench, NT-Nankai Trough, NGT-New Guinea Trench, NHT-New Hebrides Trench, PhT-Philippines Trench, PrT-Peru Trench, PyT-Puysegur Trench, RT-Ryukyu Trench, SST-South Solomons Trench, TnT-Tonga Trench (Bird, 2003).

4. Palau Digital Elevation Model Development

Land and Resource Information System Office, Palau (PALARIS) shared with PMEL the Light Detection and Ranging (LiDAR) Digital Elevation Map (DEM) with very high resolution (1 m) with Palau wide coverage. The DEM includes topography and bathymetry data up to 50 m depth. The data has gaps in deep lagoon areas (Figure 6, *a*). The additional DEMs were used to feel the gaps and add bathymetry data for the deeper ocean. Additionally, the original LiDAR data contained some remaining trees, buildings etc. that are usually removed to perform the 'bare earth' tsunami modeling. The procedure of filling the gaps and data preprocessing is described below.

The composite high-resolution DEM (modeling DEM) of Palau was created for accurate inundation modeling with consideration of all coastline, topography and bathymetry specificities (Figure 6, *b*). Table 2 summarizes the supplement DEMs used for the modeling DEM creation with its characteristics, including origin and resolutions. The DEMs are listed by usage priority. The bathymetry/topography data from Table 2 were seamlessly blended to produce a homogeneous 10 m resolution model of Palau. The MATLAB and QGIS software were used for the composite DEM creation.

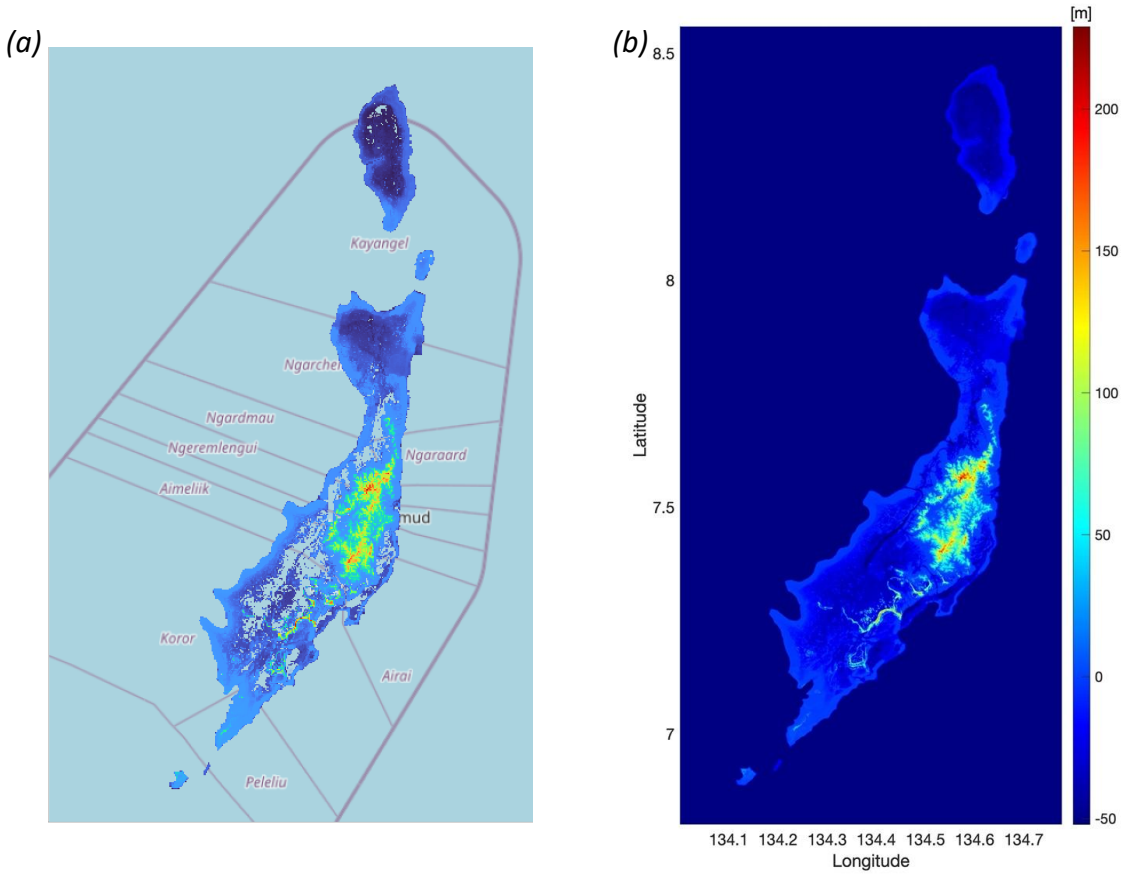

Figure 6. PALARIS LiDAR DEM with deep lagoon gaps (*a*) and modeling DEM (*b*).

Table 2: Data used for the composite Palau DEM

Number	Bathy/topo	Location	Name (Nickname)	Source	Type	Resolution
1)	Bathy and topo	Main Palau Group, where depth is up to 50 m	PALARIS LiDAR	PALARIS	LiDAR	1 m
2)	Bathy	Outer slope of Palau up to 500 m depth and deep lagoon	CRRF	CRRF [????]	Multi-beam	50 m
3)	Bathy	Main Palau group	Nautical Charts	NOAA Charts (NOAA,2024) and manual digitizing of NGA nautical charts (NGA, 2024)	Single beam, LiDAR, aerial, satellite	n/a
4)	Bathy	Deep ocean area outside main Palau group	GMRT	GMRT (Ryan et al., 2009) cleaned/curated NCEI data (NCEI, 2024)	Multi-beam and single beam	120 m
5)	Bathy	Deep ocean area outside main Palau group	GEBCO 2024	GEBCO 2024 (GEBCO,2024)	Single beam, multi-beam, satellite	15 arcsec

1). Preparing the LiDAR data for modeling. Bringing data to bare earth.

Traditionally the tsunami hazard assessment modeling is performed over the bare earth – surface of the earth excluding vegetation and manmade objects. Bare earth models represent a worst-case scenario, where there is no mitigation from natural or artificial barriers. This approach provides an upper limit to the potential inundation and wave forces, offering a conservative estimate that can inform disaster preparedness. After the detailed investigation of the LiDAR DEM, it was found that despite most of the buildings and trees being removed some structures still persist. Figure 7 *a*, *b* shows the south-west coast of Koror Island and east of the Lebugol Channel. The two marked points along the red cross section are likely trees following its dimensions and location. To remove them an algorithm based on the CSF (Cloth Simulation Filter) (Zhang et al., 2016) was applied (Figure 8). The CSF separates point clouds into ground and non-ground measurements.

To provide the upper limit of the potential inundation the tsunami modeling is performed with the MHW (Mean High Water) vertical datum. There is no a significant difference between tides in different locations in Palau, the processed LiDAR DEM was brought from the original MLLW (Mean Lower Low Water) datum to the MHW following the Malakal tide station information from the University of Hawaii Sea Level Center (UHSLC, 2024).

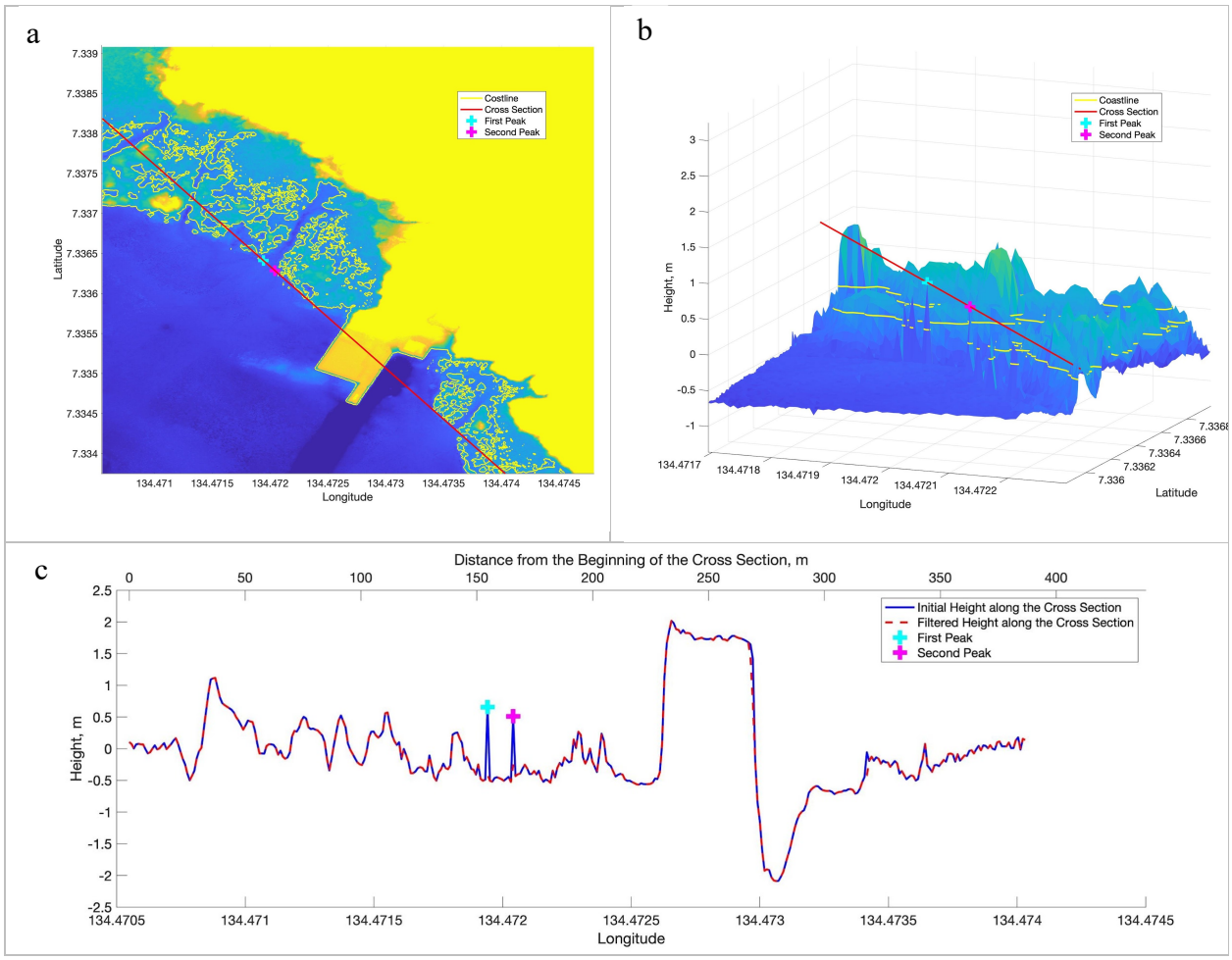

Figure 7. The south-west coast of Koror Island and east of the Lebugol Channel with the tree-like structures highlighted with the crosses along the cross section – the red line (*a*, *b*). The original DEM topo bathymetric heights along the cross section (the blue line) and the filtered heights with the structures removed (the dashed red line) (*c*).

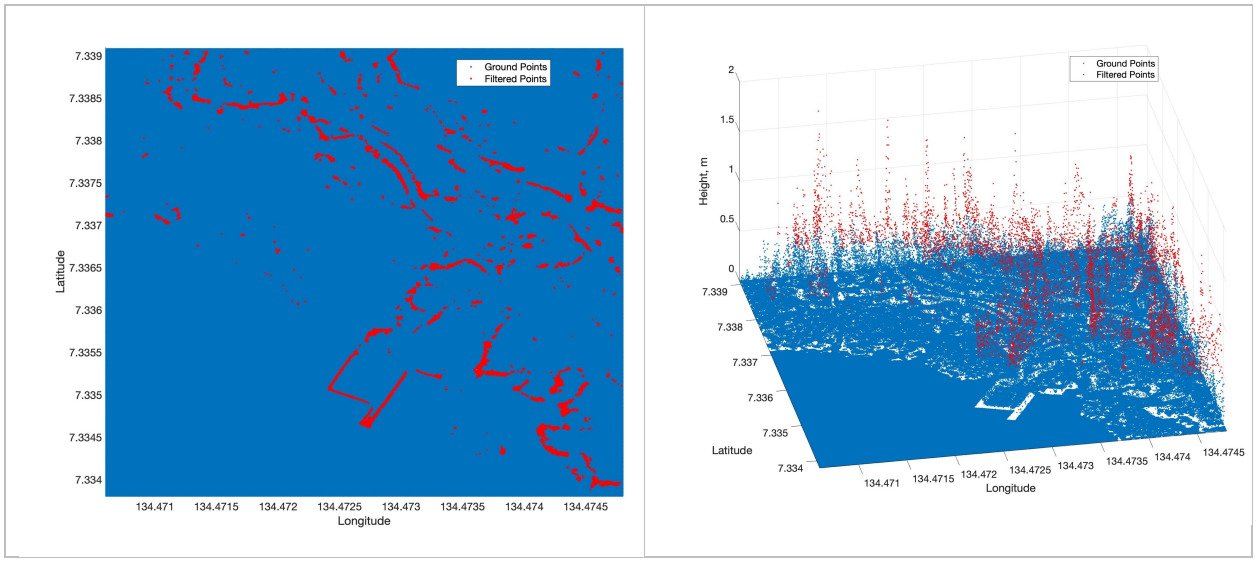

Figure 8. The application of the filtering algorithm based on the CSF. The blue dots were identified as ground points and were kept in the resulting DEM, the red dots were identified as trees or buildings and were removed from the resulting DEM.

2). The CRRF (Coral Reef Research Foundation) shared with PMEL the 50 m resolution data up to depth 500 m that consists of the multi-beam data collected and processed by the CRRF and the LiDAR data combination. We used only the CRRF data in the locations where there is no LiDAR data available. Figure 9 shows the outer slope of the barrier reef on the west of Babeldaob with the LiDAR DEM (*a*) and the CRRF dataset (*b*). The processed CRRF DEM was brought from the original MLLW datum to the MHW following the Malakal tide station information from the UHSCL (UHSLC, 2024).

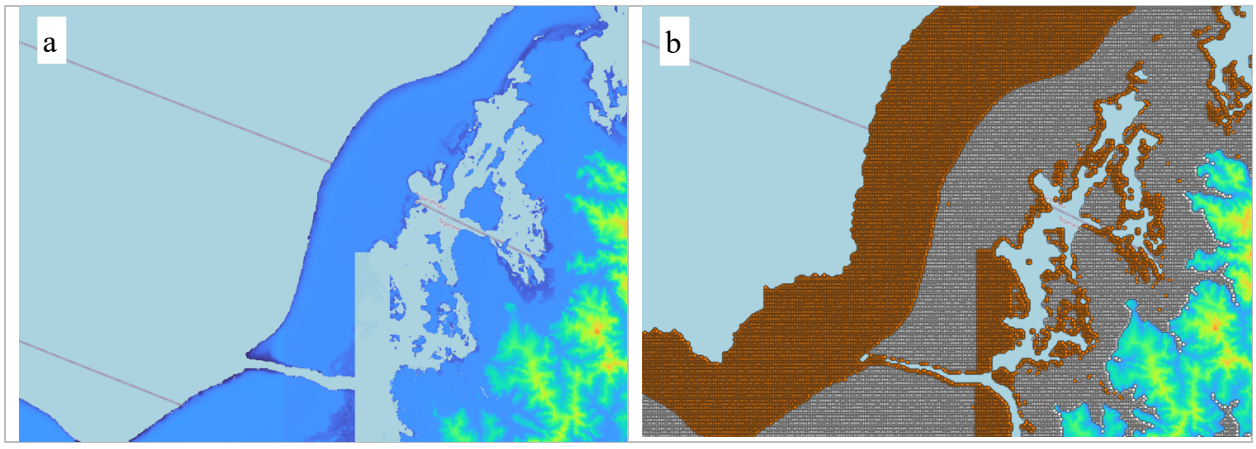

Figure 9. The LiDAR (*a*) and the CRRF multi-beam data in Toachel Mlengui (West Passage) area (*b*). Orange points indicate the CRRF data that were used and white points – the CRRF data that were not used in the modeling DEM.

3). Some gaps in LiDAR data were filled with the data from the nautical charts. The main sources for these data are the NOAA charts (NOAA, 2024) and the paper versions of the charts from the NGA (National Geospatial-Intelligence Agency) (NGA, 2024), which were manually digitized before using the data. We used only the nautical charts data in the locations where there is no LiDAR data available. Figure 10 shows the outer slope of the barrier reef on the west of Babeldaob (the same area as on Figure 9) with LiDAR data only (*a*) and LiDAR and data extracted from the nautical charts (*b*). The nautical chart data was brought from the original mean low water springs (MLWS) datum to the MHW following the Malakal tide station information from the UHSCL (UHSLC, 2024). Figure 11 shows the Malakal Harbor (*a*), Arangel Channel and Koror Road (*b*) with the LiDAR and nautical charts data inside the lagoon. The processed data was brought from the original datum to the MHW (UHSLC, 2024).

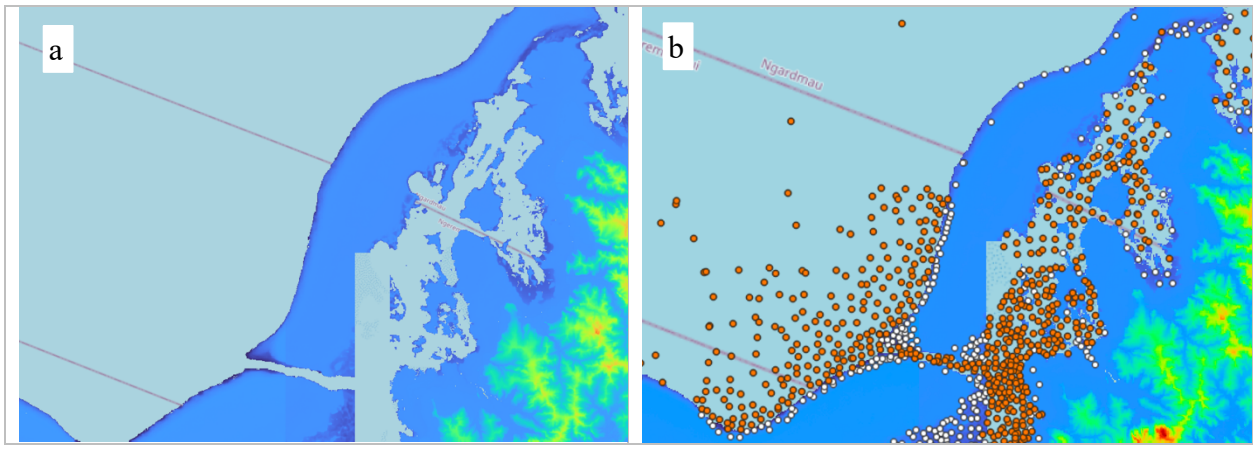

Figure 10. The LiDAR (*a*) and the nautical charts data in Toachel Mlengui (West Passage) area (*b*). Orange points indicate the nautical charts data that were used, white points – the nautical charts data that were not used.

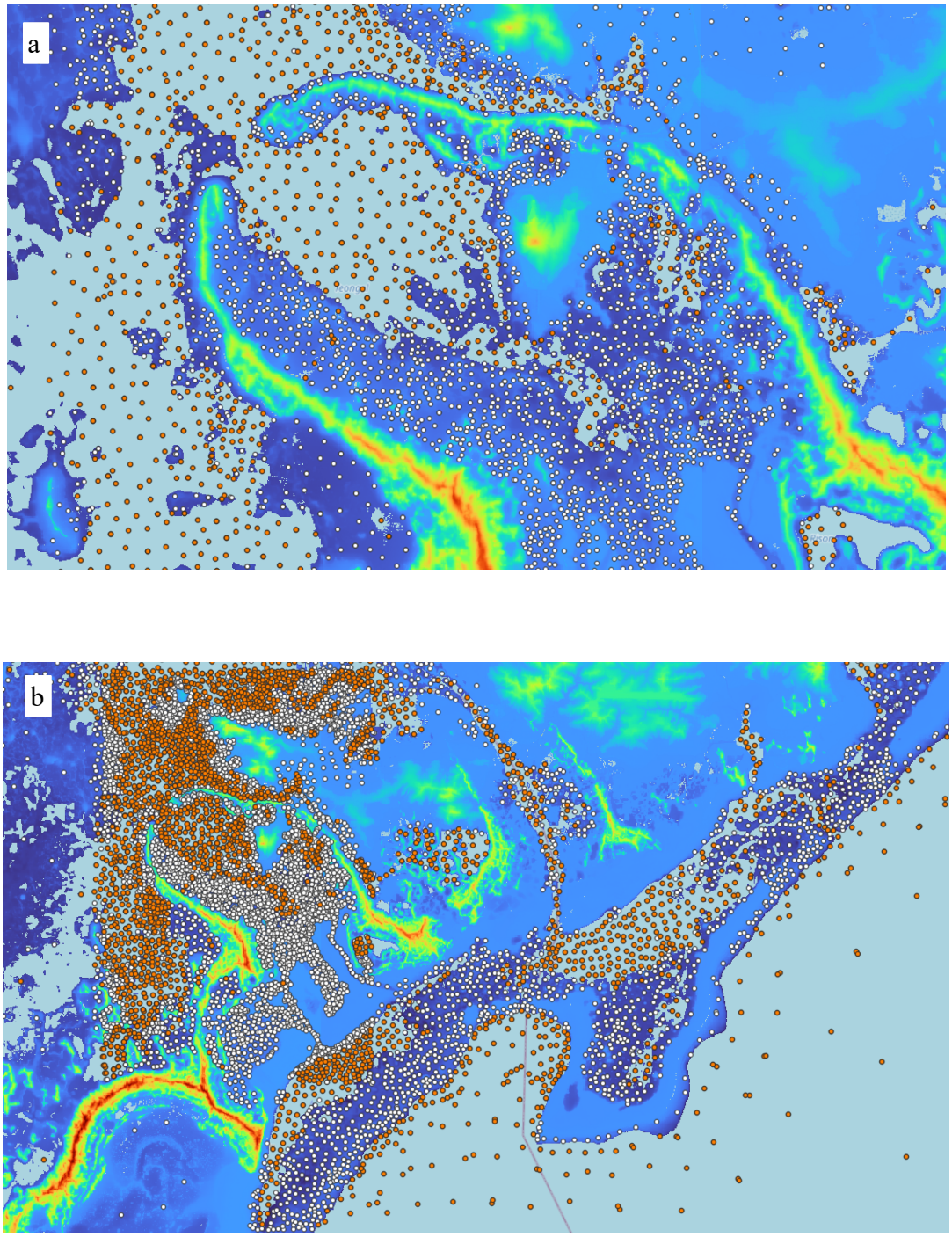

Figure 11. The LiDAR (highlighted with the colormap) and the nautical charts data (points) in Malakal Harbor (*a*), in Arangel Channel and Koror Road (*b*). Orange points indicate the nautical charts data that were used, white points – the nautical charts data that were not used in the modeling DEM.

4). The Multibeam Bathymetry Database (MBBDB) at NCEI collects and archives multibeam data from the earliest commercial installations (circa 1980) through today's modern high-resolution collections (Figure 12). Data are acquired from both U.S. and international government and academic sources and consist of the raw (as collected) sonar data files (NCEI, 2024). We used the GMRT (Global Multi-Resolution Topography Synthesis) from Lamont-Doherty Earth Observatory, where they have the cleaned/curated NCEI multibeam data (Ryan et al., 2009). We brought the GMRT data from the Mean Sea Level (MSL) to the MHW and kept only the data outside the Main Palau Group polygon.

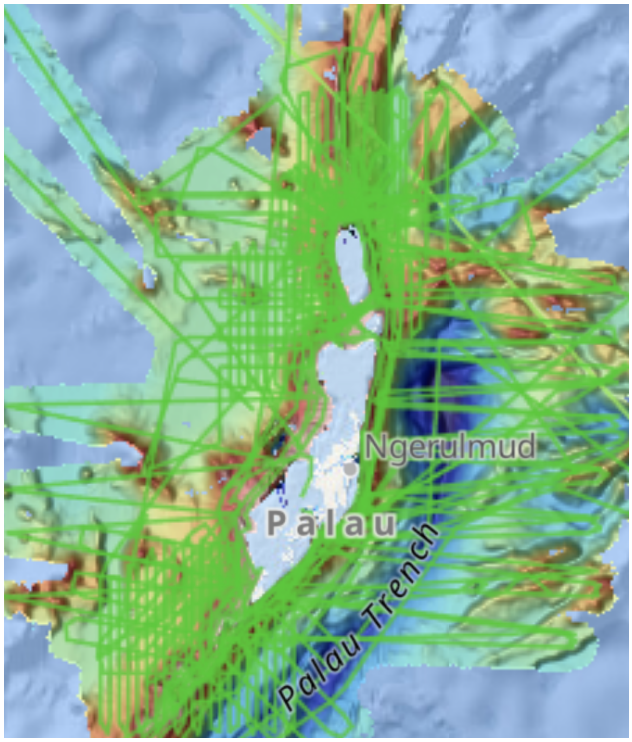

Figure 12. Ship tracks of the multibeam bathymetric surveys archived at NOAA NCEI with shaded-relief imagery on the back plan.

5). GEBCO's current gridded bathymetry data set, the GEBCO_2024 Grid, is a global terrain model for ocean and land, providing elevation data, in meters, on a 15 arc-second interval grid. The data is the combination of ship-based measurements, satellite data, and crowdsourced contributions. We used the GEBCO dataset only outside the Main Palau Group, where there is no other bathymetry data available. Figure 13 shows the combination of the GMRT and GEBCO data outside the Main Palau Group.

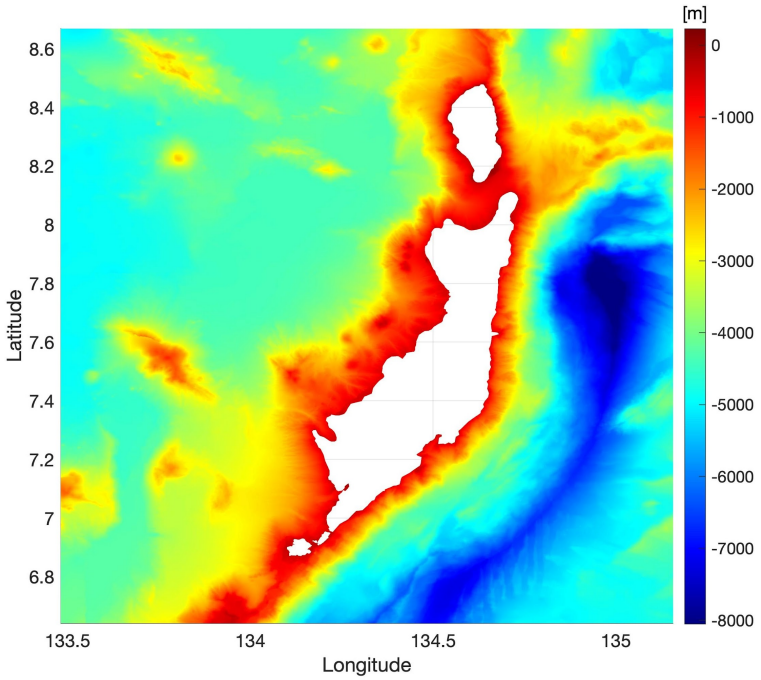

Figure 13. The combination of the GMRT and GEBCO data outside the Main Palau Group.

All the prepared datasets described in 1 – 5 were seamlessly blended to produce a composite, homogeneous, regular 10 m resolution model of Palau appropriate for accurate inundation modeling with consideration of all coastlines', bathymetric and topographic specificities.

5. Tsunami Model and Grid Development

Due to a recent collaboration with the University of Malaga, Spain, the NOAA Center for Tsunami Research (NCTR) has access to a relatively new model, HySEA – an NTHMP-benchmarked inundation model. The benchmarking involves extensive testing against a number of theoretical, laboratory, and field data summarized in Synolakis et al., 2008 and NTHMP, 2017. This tsunami model code has been designed to solve the nonlinear shallow water equations and utilizes GPU graphics cards for parallelization, making it suitable for very large, very high-resolution grids. The HySEA model was earlier validated against the MOST model used in the operational forecasting of tsunami inundation at NOAA's Tsunami Warning Centers on tsunami modeling in a study conducted for the U.S. Virgin Islands: St. Thomas, St. John, and St. Croix (Moore and Arcas, 2019). In addition to the seismic parameters to determine the initial deformation, digital elevation models (DEMs) are required to run HySEA.

The nested grids are implemented in the HySea model keeping the accuracy-speed balance. Three levels of larger grids contain these highest-resolution grids, in increasing size and

resolution. The HySEA model requires resolution "jumps" between these nested grids only by factors of 2, 4, 8 or 16.
HySEA is a finite-volume numerical model and has grid-alignment nesting requirements that ensure that volume centroids for each cell fall exactly on the cell location for inner grids in the nesting (Figure 14). This requirement, along with the desire not to re-interpolate the source DEM means that the innermost grids be developed first by determining extent and ensuring that each successive outer grid has resolutions that are integer-multiples of inner grids.

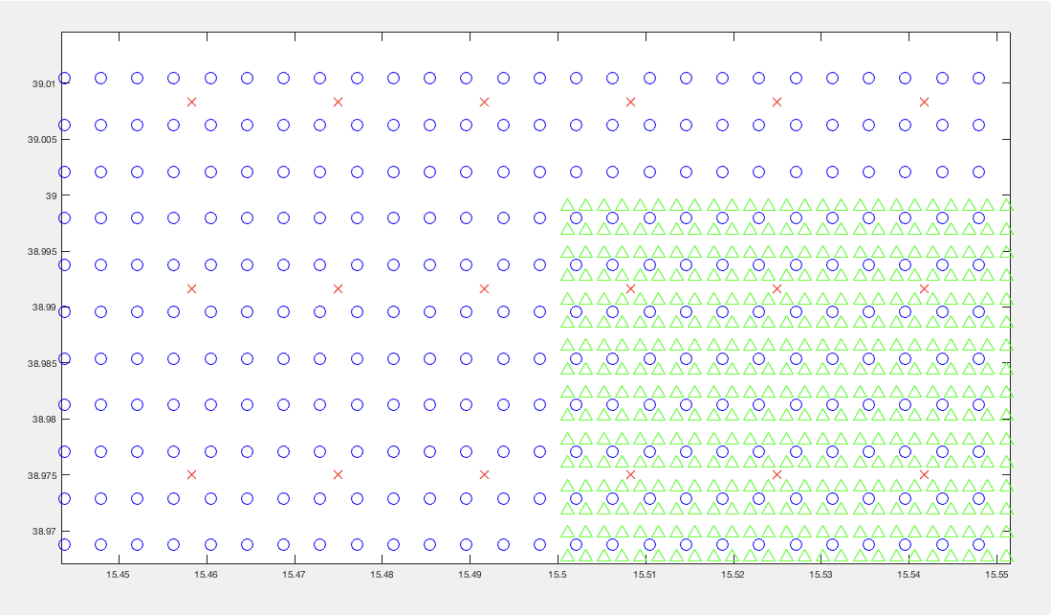

Figure 14. Grid nesting for HySEA showing innermost grid points (green) of twice the resolution of intermediate grid points (blue). Intermediate points have four times the resolution of outermost grid points (red) from Moore and Arcas (2019).

The grid resolutions are shown in Figure 15, innermost (red frame) 0.324 arc-seconds, intermediate (yellow) 2.592 arc-seconds, regional (green) 20.736 arc-seconds, and outermost (magenta) 82.943 arc-seconds. The ratios between resolutions are, therefore, 8, 8, and 4, respectively. A separate optimized grid was created for sensitivity study described below with grid resolutions 3.239, 12.957, 51.828 and 207.313 arc-seconds correspondingly. The ratios between resolutions are, therefore, 4, 4 and 4, respectively. Palau composite (modeling) DEM was used for the innermost and intermediate grids, publicly available elevation (including ocean and land) 15 arcsec dataset GEBCO (GEBCO, 2024) was used as the source DEM for the regional and outermost grids.

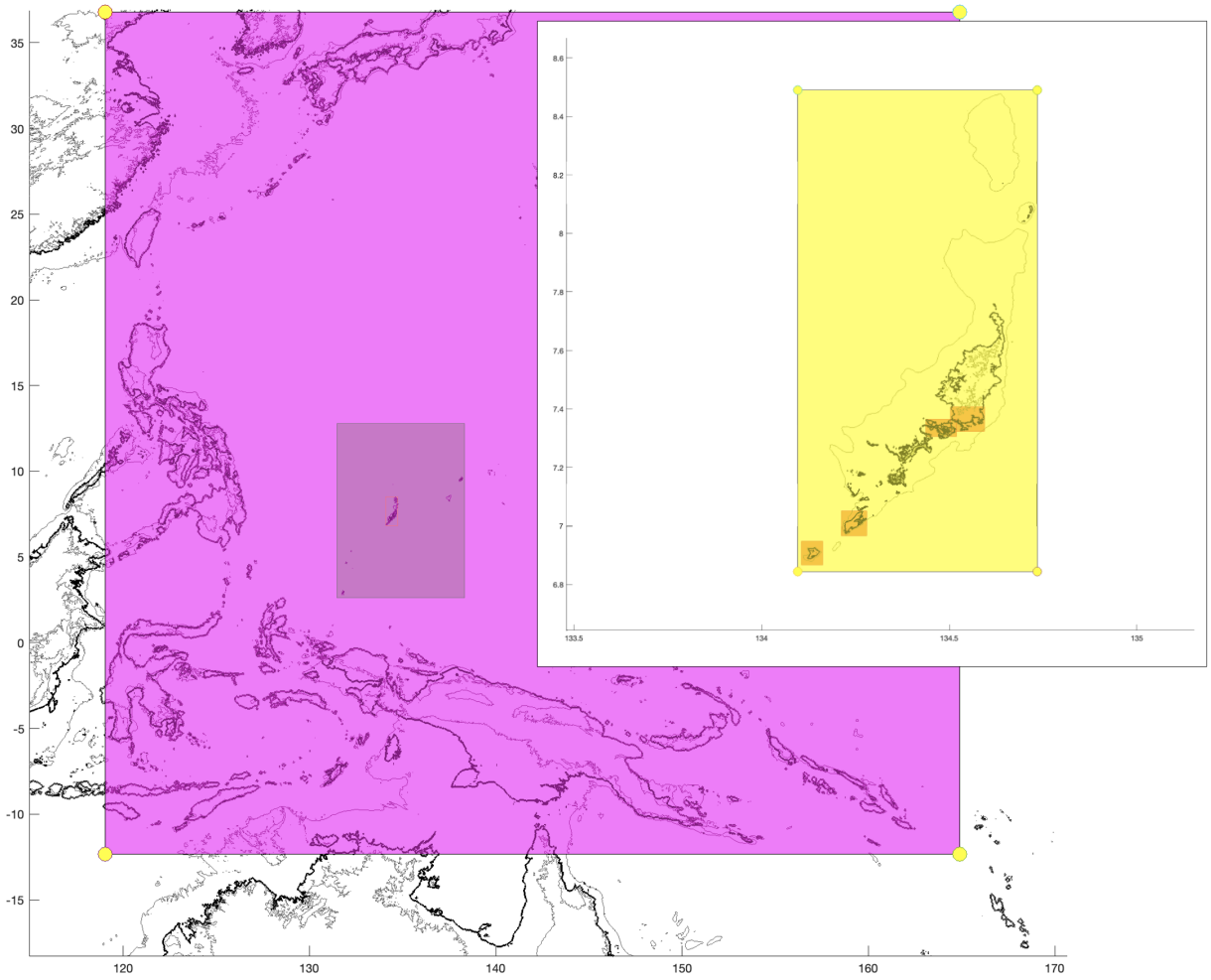

Figure 15. Extents of the grids: outermost (magenta) encompasses the nearby SZs and all inner grids, the intermediate (green) includes Southwest Islands of Palau and Yap (The Federated States of Micronesia), the next level (yellow) includes the Main Palau Group, and the innermost grids (red frame) includes Angaur, Peleliu, Koror and Airai states of Palau.

6. Tsunami Source Scenarios

For tsunami hazard assessment we use a scenario-based assessment technique based on credible worst-case tsunami events. To identify the most hazardous sources, we conducted a sensitivity study using tsunami modeling on optimized grids from the megathrust earthquakes with the 2,500-year return period. We considered SZs that have the historical recordings of tsunami ever affecting Palau (Philippine, New Guinea, Japan, Kuril-Kamchatka Trenches) and located close to Palau SZ that have a potential to affect it significantly (Palau, Yap, Mariana, Izu-Bonin, Mariana, Ryukyu Trenches and Nankai Trough). The earthquake scenarios identified in the sensitivity analysis as most hazardous were modeled at the highest possible resolution of 10 m.

6.1 Maximum magnitude assessment and propagation database

Based on the historical cases and the Palau geographics we considered only earthquake-generated tsunami. For the worst-case tsunami hazard assessment, we evaluated the maximum potential earthquake magnitude for each subduction zone, using a 2500-years return period. The 2500-years return period, that corresponds to 2% event probability in 50 years (0.04% annual probability), is a common standard used in tsunami hazard assessments, in engineering and urban planning, particularly for critical infrastructure (e.g., nuclear power plants, dams, and coastal defenses). This return period is chosen based on the need to understand and plan for catastrophic events that could have major consequences for infrastructure, population safety, and risk management. We based our estimations of maximum amplitudes on Schäfer and Wenzel, 2019. In average the results of this study find themself as a top-end mean estimate among other studies (Rong et al., 2014, McCaffrey, 2008, Berryman et al., 2015 and Davies et al., 2017). The maximum earthquake magnitudes (Mw) with the 2500-years return period corresponding to considered in this study SZ are summarized in the Table 3:

A pre-computed propagation database consisting of water level and flow velocities at all grid points for potential seismic unit sources has been developed for the world ocean basins by the NOAA Center for Tsunami Research (Gica et al., 2008). Subduction zones have been broken into finite fault segments, or unit sources, each measuring 100 km long by 50 km wide (Figure 16). The propagation database represents a composite from each of these discrete earthquake rupture segments by computing wave propagation throughout the entire Pacific Basin. Each unit source is equivalent to a deformation due to an earthquake with a fault length of 100 km, fault width of 50 km, and a slip value of 1 m, equivalent to a moment magnitude of 7.5. Larger events are modeled by combining unit sources. A Mw 9.1 event, therefore, can be successfully modeled as a 700 km × 150 km rupture with a 12 m slip, effectively a combination of 21 Mw 7.5 events scaled up 12 times. The rupture length and width are calculated from Mw using the empirical relationships from Wells and Coppersmith (1994) and slip from Hanks, T.C., & Kanamori, H. (1979). The maximum earthquake magnitudes (Mw) with the 2500-years return period for each considered in this study SZ and corresponding rupture length, width and slip are presented in the Table 3. For example, the Mw 8.5 tsunami source originated from the Philippine Trench has 300 km length, 100 km width and 6 m slip and is formed by six-unit sources 100 km long by 50 km wide (3 × 2 blocks) (Figure 17). In the sensitivity study all the sources consisting of the consecutive 3 × 2 blocks were tested. 20 sources originating from the Philippine Trench were tested (Figure 17, *b*).

Table 3: SZs maximum amplitudes with the 2500 years return period and the corresponding tsunami sources sizes and slips

SZ	Max Mw 2500 yr	Source Size (km)	Slip (m)
Philippine Trench	8.5	300 × 100	6
New Guinea Trench	8.2	200 × 50	5
Palau Trench	7.4	100 × 50	0.8
Yap Trench	7.8	100 × 50	3.2
Mariana Trench	8.4	300 × 50	7
Izu-Bonin Trench	8.6	400 × 100	5
Japan Trench	9.1	700 × 150	12
Kuril-Kamchatka Trench	9.0	600 × 100	15
Ryukyu Trench	8.5	300 × 100	6
Nankai Trough	9.0	600 × 100	15

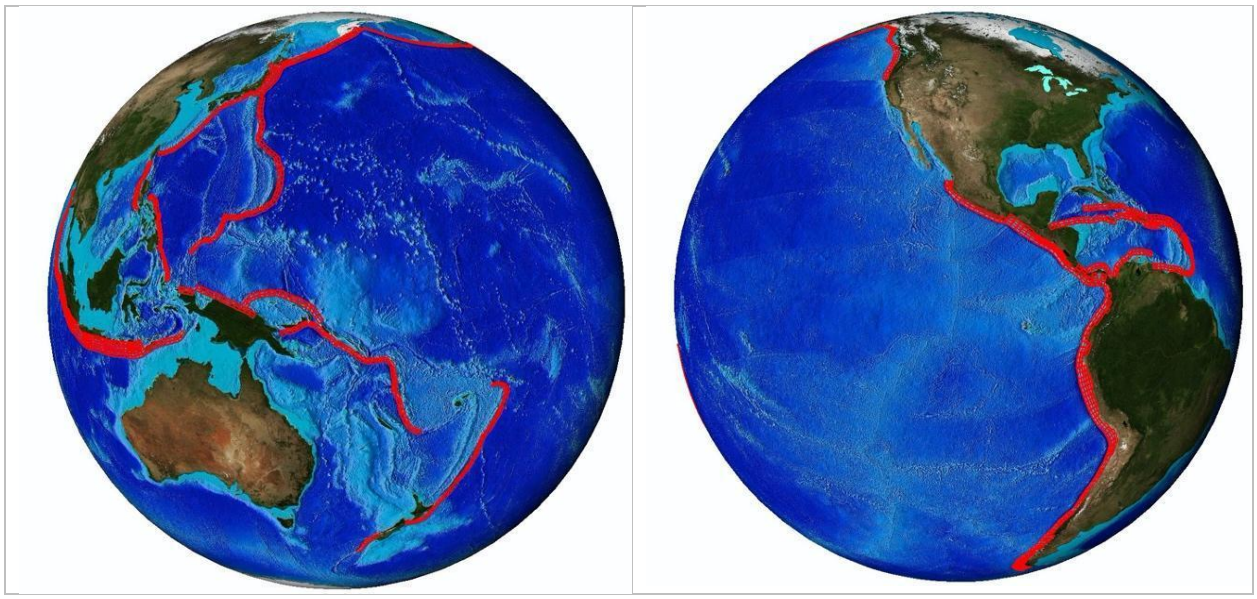

Figure 16. Locations of the unit sources for pre-computed simulated earthquake events in the Propagation Database. These can be combined to provide a very fast forecast during an actual tsunami event.

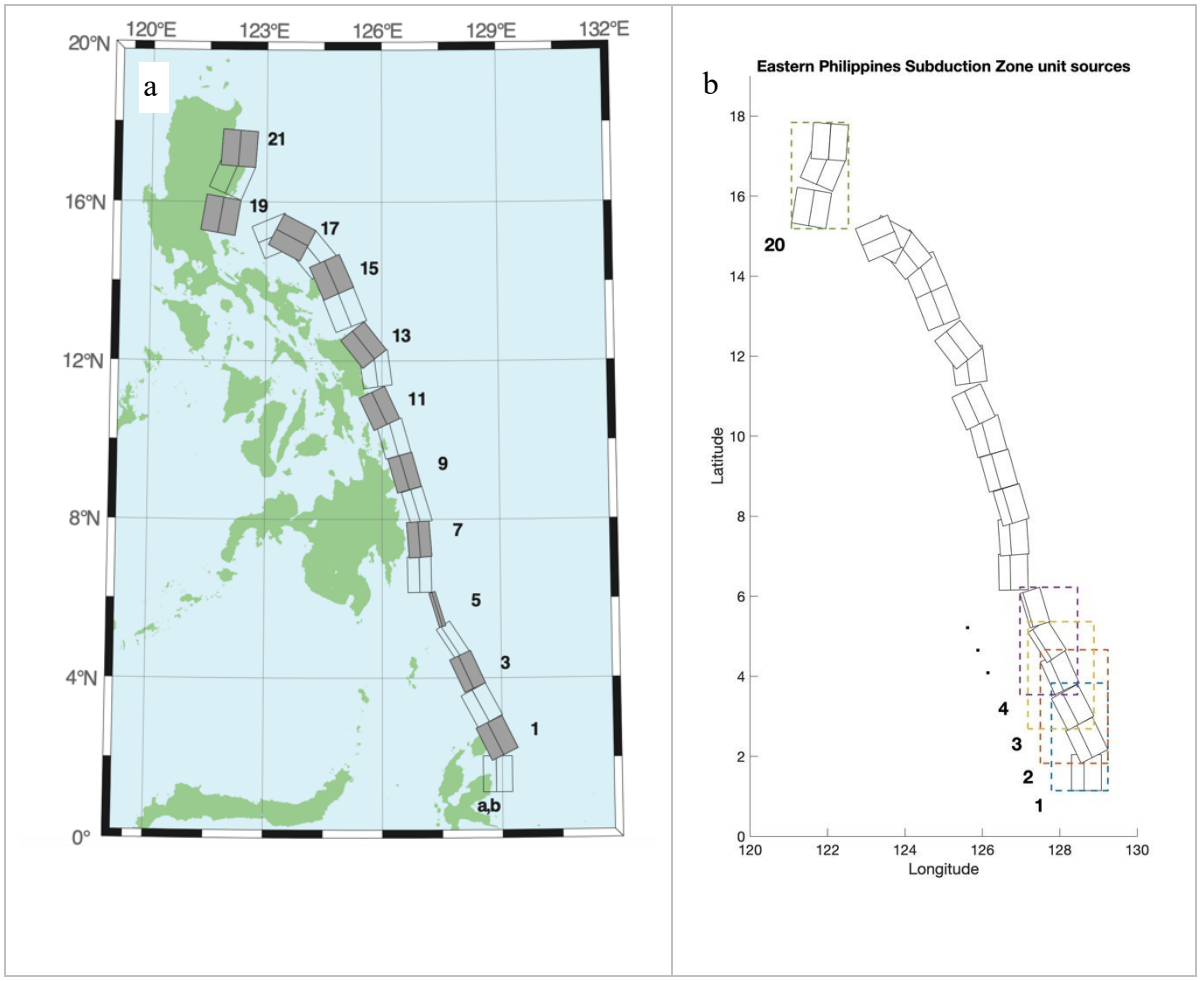

Figure 17. The Philippines Trench subdivision into the unit sources following Bird (2003) (*a*) and synthetic Mw 8.5 sources (*b*).

Tsunami energy radiating away from a source is highly directional and depends on source characteristics and bathymetry. Each tsunami event has its specific complex pattern of tsunami amplitudes, arrival times, and
frequency decay. Previous studies have shown that tsunamis triggered by similar magnitude earthquakes along
different subduction zone sources may have substantially different impacts on the same site (Uslu (2009), Dengler et al. (2008)). With this source dependency in mind, a comprehensive sensitivity study was performed to determine potential earthquake-generated tsunami source regions of greatest concern to the Main Palau Group.

In the sensitivity study 138 synthetically generated tsunami sources were modeled with computationally optimized grids (nested grids ~ 3.239, 12.957, 51.828 and 207.313 arc-seconds).

Gica et al. (2008) provide detailed descriptions of all unit sources with tabulated source parameters for each unit source, including their locations (longitude and latitude), focal depths, strikes and dips. The rake angles are all set
to 90° for all unit sources.

6.2 Sensitivity testing

A tsunami hazard assessment for the Main Palau Group was conducted first by investigating its sensitivity to tsunami impact from the 138 earthquake-triggered tsunami scenarios. Figure 18 shows the sensitivity testing results: maximum tsunami heights at Palau calculated from all synthetic sources on an optimized grid. From the consecutive sources the color of the first two blocks along the fault width identifies the maximum run-up caused by the whole source. For example, for the Philippine Trench the color of the unit sources 1a and 1b (Figure 17, *a*) is green (Figure 18), that means that the maximum tsunami run-up to Palau from the synthetic source consisting of unit sources 1a, 1b, 2a, 2b, 3a, 3b is more than 1.5 m and less than 3.5 m – 3.2 m. Model results show that maximum wave run-ups happen from sources along the Philippine Trench and reach 8 m and above (Figure 18). Earthquakes in these regions, therefore, pose the greatest potential tsunami hazard to Palau, determined by the distance to the source and direction of the most energy released.

We focus on the most hazardous sources as they provide the largest inundation, but it is possible that smaller events inundate an area that a larger source has not, either because the incident direction of wave fronts from the two sources come from different directions, or because the dynamics of the wave as it shoals causes a focusing specific to a certain source. Based on this consideration, subsequent to the sensitivity study, we selected four earthquake scenarios to be modeled at the highest resolution of 10 m: two the most hazardous to Palau sources along the Philippine Trench and two closest to Palau sources with the significant impact (one source from Palau and one from Yap Trenches). The Philippine Trench sources and Yap-Palau Trench sources are located on opposite sides of Palau. Table 4 provides the scaling parameters used for the NOAA propagation database for these four sources. Following the sensitivity testing the tsunami originated from the Philippine1 source has the biggest run-up height on the Main Palau Group and the Philippine2 source has the biggest run-up height on Koror coastline and the second biggest on the Main Palau Group.

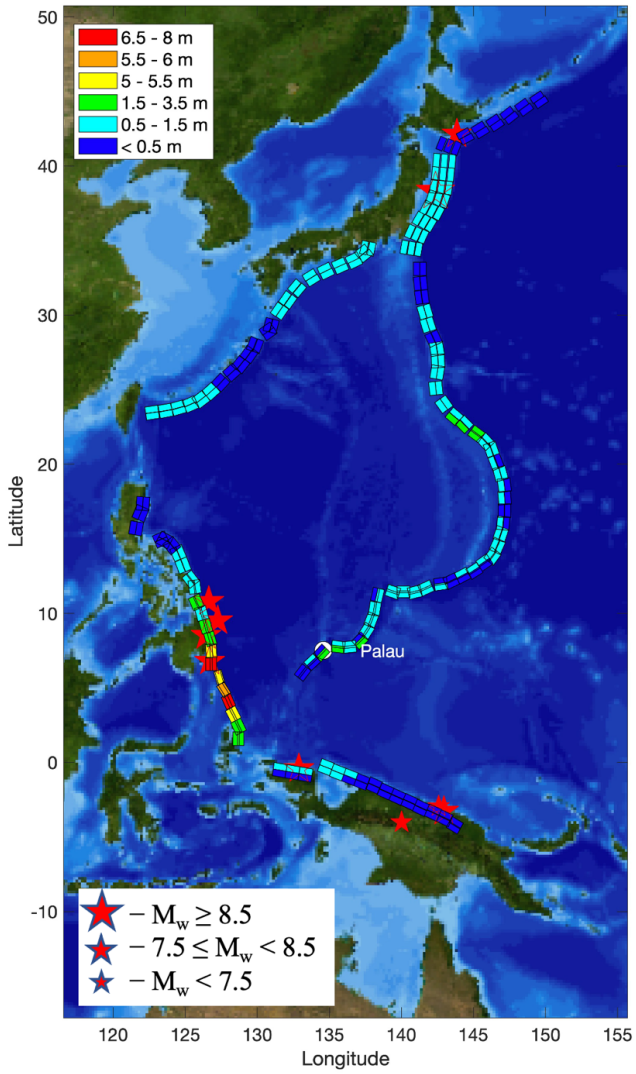

Figure 18. Maximum tsunami heights computed for Palau Main Group from tsunamis triggered by synthetic earthquakes around Pacific Basin subduction zones. The optimized grids were used for all model runs.

Table 4: Unit sources forming two most hazardous sources (from the Philippine Trench) and two closest sources, causing the significant impact (from the Yap-Palau Trench). The notation follows Bird (2003)

Source Nickname and Subduction Zone Origin	Tsunami Source from Unit Sources
Philippine1	6*ep3a+6*ep3b+6*ep4a+ 6*ep4b+6*ep5a+6*ep5b
Philippine2	6*ep6a+6*ep6b+6*ep7a+ 6*ep7b+6*ep8a+6*ep8b
Yap	3.2*ki72b
Palau	0.8*ki73b

7. Model Validation

Two tsunami records at the Malakal tide gauge are available: one from the 10 March 2011 Tohoku and another one from the 2 December 2023 Mindanao earthquakes. Table 5 provides information on the earthquakes along with the tsunami source scaling parameters from the NOAA propagation database. Figure 19 shows the computed maximum wave amplitudes in deep ocean (*a*), in Palau (*b*) and the comparisons of the calculated and observed water level variations at the Malakal tide gauge (*c*) from the 2011 Tohoku tsunami. Figure 20 shows the computed maximum wave amplitudes in deep ocean (*a*), in Palau (*b*) and the comparisons of the calculated and observed water level variations at the Malakal tide gauge (*c*) from the 2023 Mindanao tsunami. Any discrepancies between the calculated and observed sea level variations are mostly due to the source uncertainties.

Table 5: Parameters of the 10 March 2011 Tohoku and the 2 December 2023 Mindanao earthquakes and corresponding unit sources forming the sources

Data	Time (UTC)	Location	Epicenter	Mw	Tsunami Source from Unit Sources
2011-03-11	05:46:24	Japan	38.322°N 142.369°E	9.0	6.31*ki25a+1.91*ki25b+27.39*ki26a+0.48*ki26b+ 17.5*ki26y+20.99*ki26z+17.01*ki27a+12.43*ki27z+ 4.14*ki28z+9.54*ki29a
2023-12-02	14:37:04	Philippines	8.527°N 126.416°E	7.6	0.371*ep8a + 0.598*ep8b

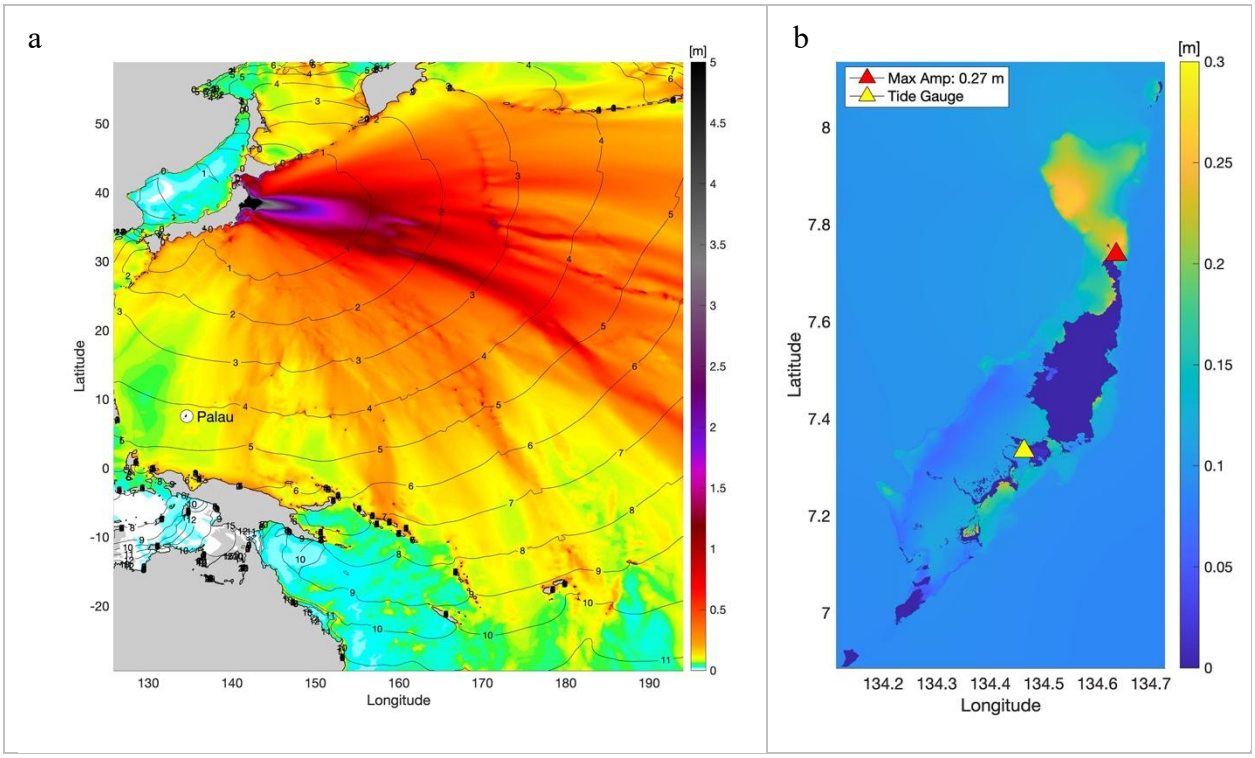

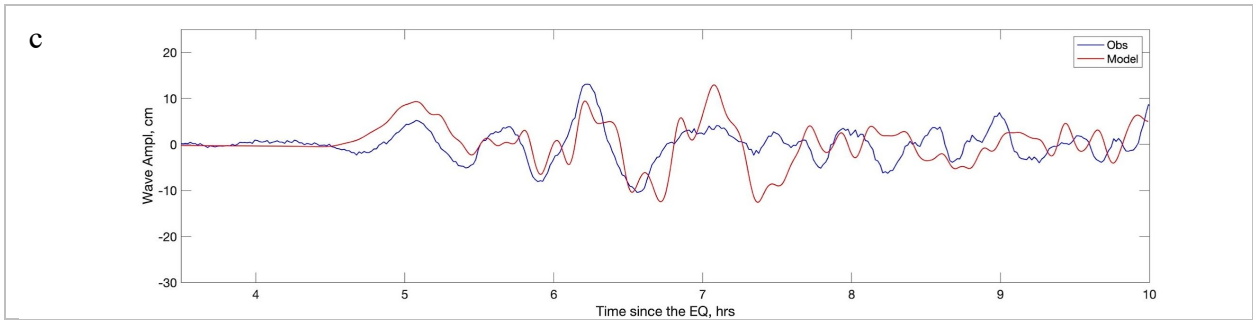

Figure 19. The computed maximum wave amplitudes in deep ocean (*a*), in Palau (*b*) and the comparison of the calculated and observed water level variations at the Malakal tide gauge (*c*) from the 10 March 2011 Tohoku tsunami.

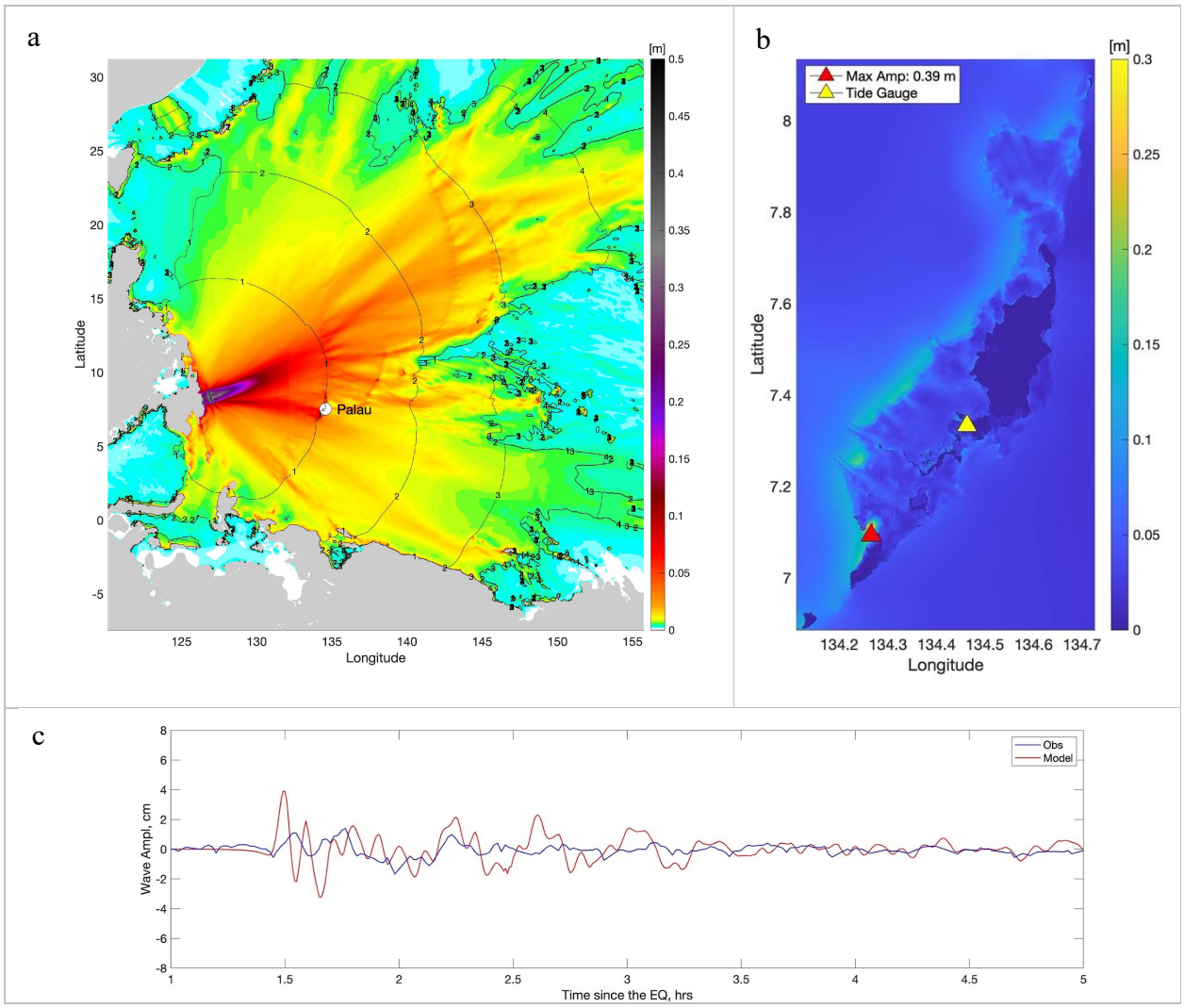

Figure 20. The computed maximum wave amplitudes in deep ocean (*a*), in Palau (*b*) and the comparisons of the calculated and observed water level variations at the Malakal tide gauge (*c*) from the 2 December 2023 Mindanao tsunami.

8. Modeling Results

HySEA was run for each of the four sources described in Section 6. The outputs of HySea include tsunami travel time (arrival time), maximum amplitude (tsunami height), flow depth, current speed and current attenuation. In deep ocean, the travel time and maximum amplitude are determined, while in the Palau grid, the travel time, tsunami height, flow depth, inundation, current speeds and current attenuation are determined.

Maximum amplitude is the highest elevation reached by seawater measured relative to a stated datum, high water for this study. Tracking the maximum wave amplitude over all the time steps of a model run gives the largest height for a given source at all locations on the grid. Maximum wave amplitudes for the whole simulation were saved at every grid point every 60 seconds in order to produce inundation maps. Tsunami heights and current speeds were saved at the most populated locations and locations with important infrastructure. Wave amplitudes were also saved every 60 seconds for the first five hours of the simulation at every grid point for the most hazardous source for Palau Philipine2 to track the tsunami wave dynamics.

Figure 21 shows the source location, arrival times (travel time isochrones), and maximum wave amplitudes in the deep ocean in the propagation phase for the four sources modeled. In these figures, it is also possible to appreciate the directionality of the modeled tsunamis. Figure 21 *a*, *b* highlights the sources Philippine1 and Philippine2 that cause the largest run-ups at Palau. Tsunami from these sources reach Palau barrier reef ~45 minutes from the earthquake. The tsunami from sources Yap and Palau are significantly smaller, but the waves will reach Palau within minutes after the earthquake (Figure 21 *c*, *d*), so education, planning, preparedness and mitigation are fundamentally necessary. It is important to get the local communities advised about the possible impact and get prepared.

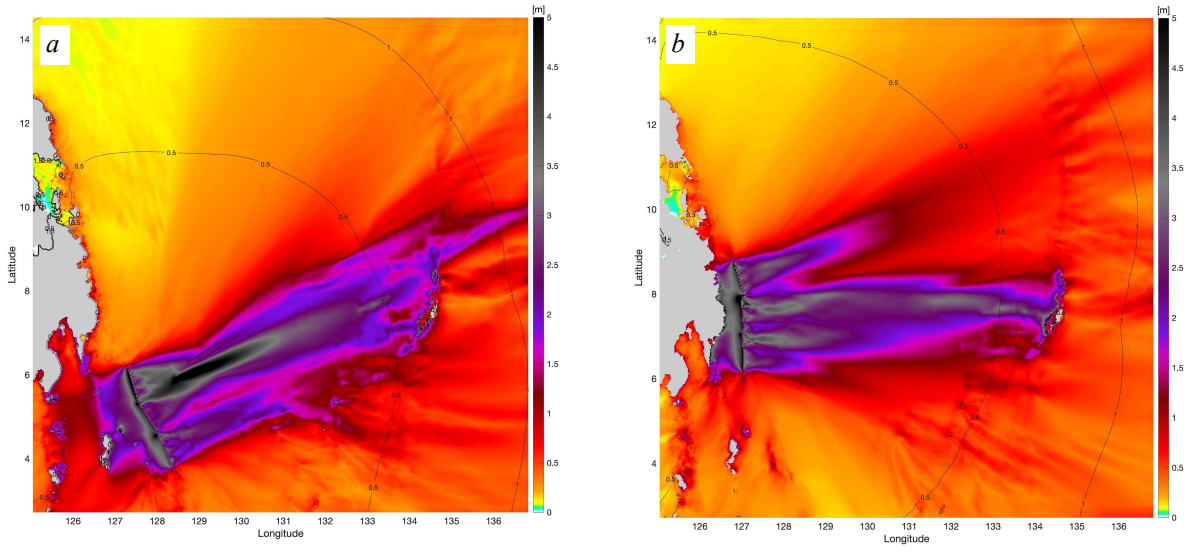

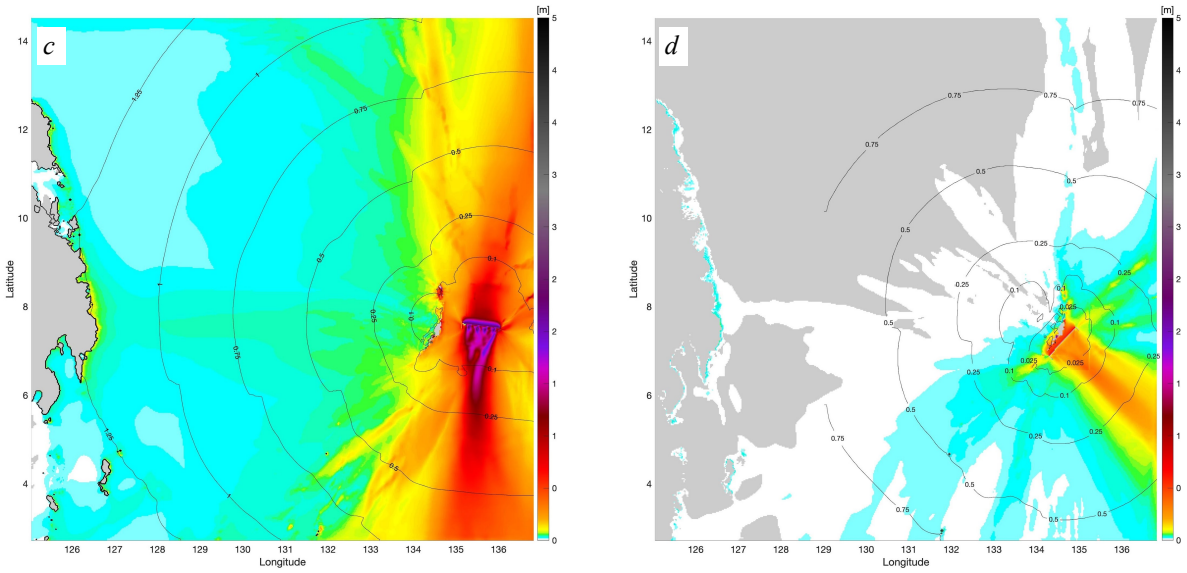

Figure 21. Source location, arrival times, and maximum wave amplitudes in deep ocean from the most hazardous sources Phillipine1 (*a*), Philippine2 (*b*) and the closest to Palau sources with significant impact Yap (*c*) and Palau (*d*).

Once the tsunami reaches Palau, the inundation phase and offshore currents are modeled. The term tsunami height is used to indicate the elevation above sea level (analogous to amplitude in the open ocean). When the tsunami height is larger than the ground elevation there is inundation. The inundation area is defined by all the areas where the tsunami height is larger than ground elevation. The maximum tsunami height may be located anywhere in the inundation area, while run-up is the ground elevation at the limit of tsunami inundation, sometimes they coincide. Flow depth is the height of the tsunami above the ground elevation, or the depth of water a person, building or object in the flood zone experiences (Figure 22).

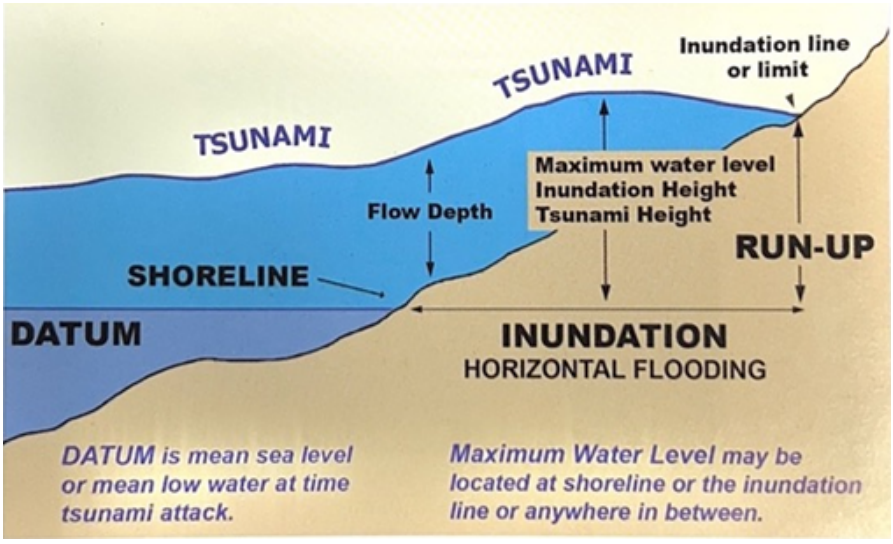

Figure 22. Tsunami inundation terms (Intergovernmental Oceanographic Commission, 2019).

Maximum current speed for the whole simulation was saved at every grid point every 120 seconds and every 60 seconds for the first five hours of the simulation at every grid point for the most hazardous source for Koror – Philippine2. Figure 23 illustrates maximum wave amplitudes and tsunami heights, as well as currents (black vectors) at different times from the most dangerous source for Koror, Philippine2.

8.1. Wave Arrival

Figure 23 also shows the tsunami in Palau at different times from earthquake origin for the Philippine2 source which is the most dangerous for Koror coastlines. The wave arrives from the west starting with the rise of water (runup) and reaches Angaur and Peleliu first (*a*). When the tsunami reaches the barrier reef it slows down and increases in height (*b*). Further it partly reflects from the reef and partly penetrates to lagoon through the passes and reefs, the current velocities are the biggest in narrow passes (*b*, *c*). The velocity vectors show the wave refracts around the lagoon and gets inside it from the opposite to the source – east side of the Main Palau Group. The waves continue propagation and refracting inside the lagoon slower than in deep ocean due to the shallow depth and multiple obstacles (*d, e*). Approximately one hour and 15 minutes after the earthquake it reaches Koror. Three hours after the earthquake the wave mostly leaves the lagoon (*f*).

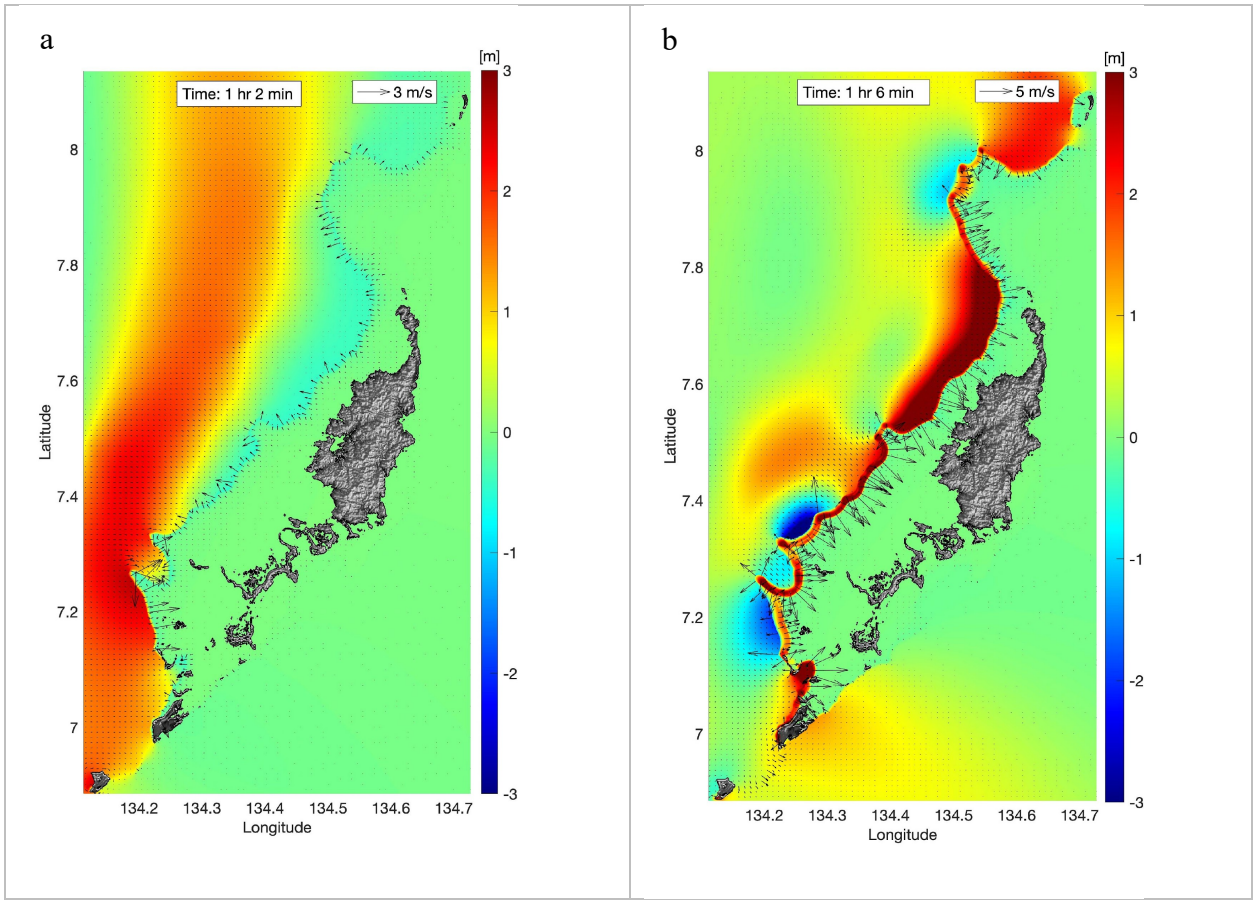

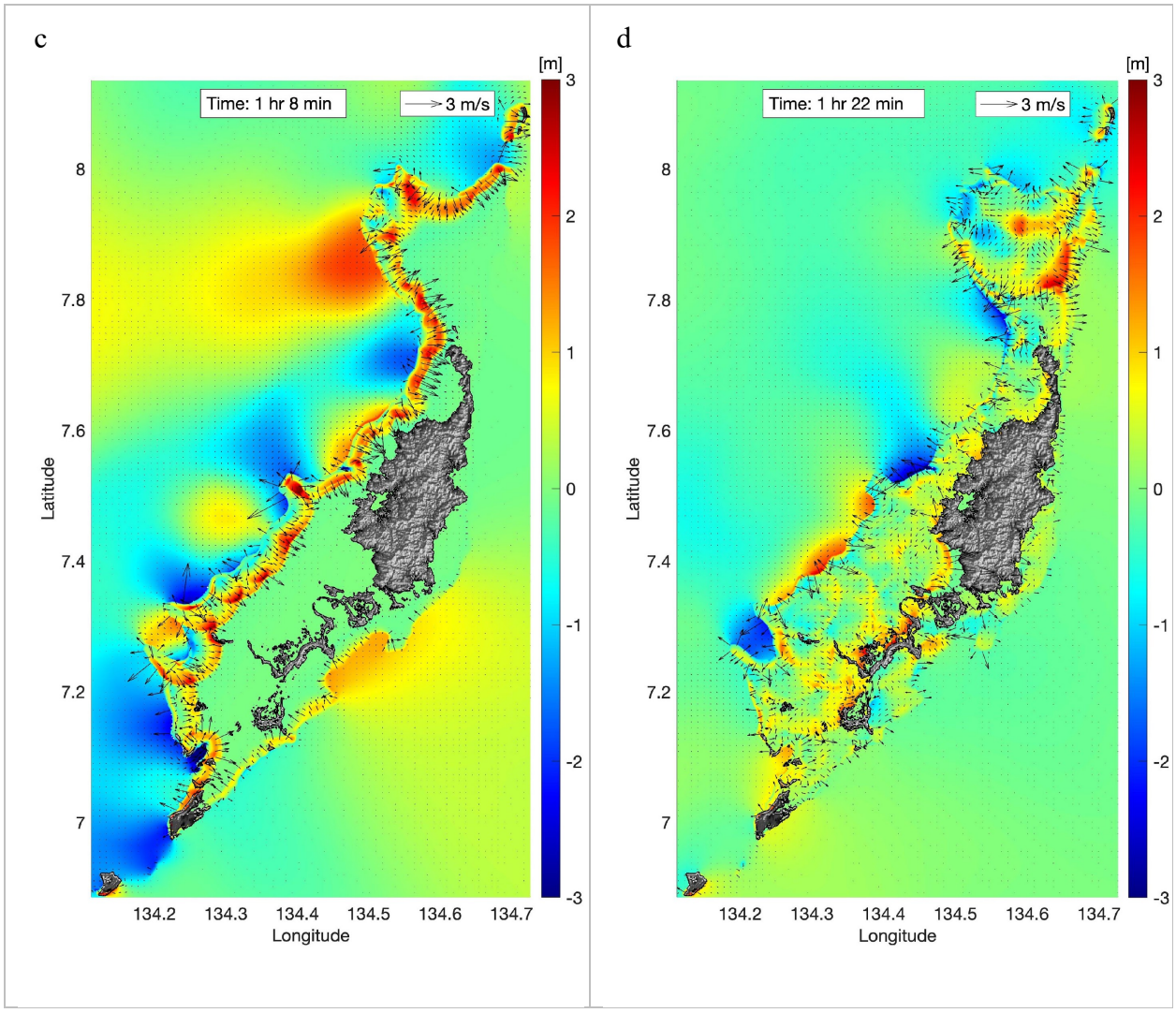
c
Time: 1 hr 8 min
3 m/s
[m]
3
2
1
0
-1
-2
-3
8
7.8
7.6
7.4
7.2
7
Latitude
134.2
134.3
134.4
134.5
134.6
134.7
Longitude
d
Time: 1 hr 22 min
3 m/s
[m]
3
2
1
0
-1
-2
-3
8
7.8
7.6
7.4
7.2
7
Latitude
134.2
134.3
134.4
134.5
134.6
134.7
Longitude

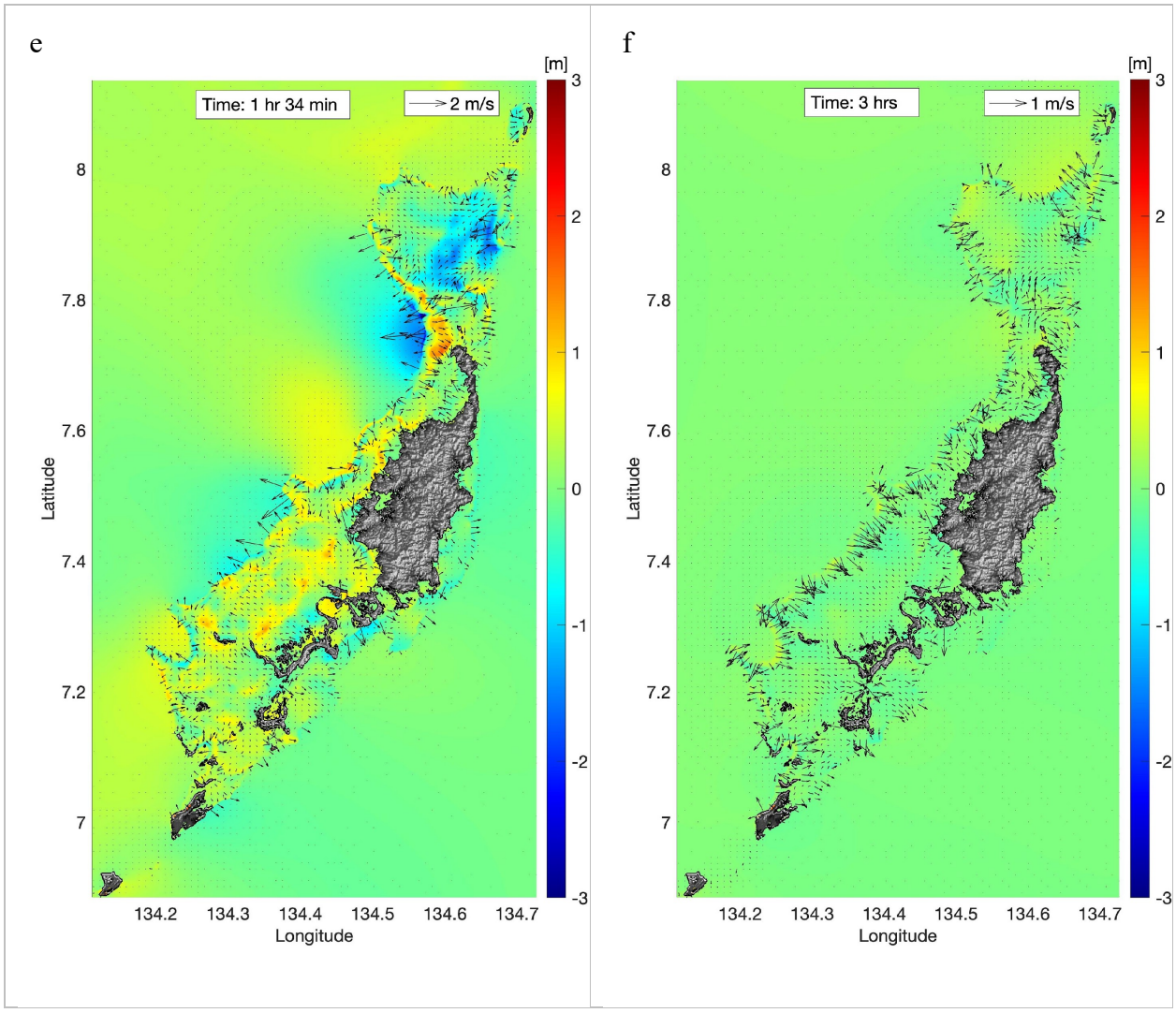

Figure 23. The wave amplitudes (offshore) and tsunami heights (onshore) and currents (black vectors) at different times after the earthquake (shown on figures) from the Philippine2 source, the most dangerous for Koror. The current scaling is in the upper right corner of each figure.

8.2 Maximum Tsunami Height, Inundation, Runup, and Flow Depth

Maximum tsunami height, inundation, runup and flow depth were determined for all of the Main Palau Group consisting of 14 States of Palau shown on Figure 24. Figures 25 and 26 illustrate the maximum wave amplitudes and tsunami heights from the two most hazardous sources for Palau: Philippine1 (Figure 25, the first column) and Philippine2 (Figure 25, the second column) for each state. The largest values for maximum tsunami height are 11.08 m and 8.9 m respectively in the north of Carp Island, Peleiu State. The biggest tsunami run-ups with extensive inundations are observed in Angaur and Peleiu states due to the shorter distance to the source and lesser reef protection than other states. Most of the west coast states of Babeldaob and Koror experience the biggest run-ups from tsunami originating from the Phillipine2 source and the east coast states – from the Phillipine1 source. In general, the low-lying beaches get the biggest inundation.

The tsunami inundation and run-ups from Yap and Palau sources are less. Figure 27 shows only the states where the run-ups are bigger or comparable with run-ups from the Philippine Trench sources. We consider these sources because these are short distances from Palau, have a significant impact on some states and are located on the opposite side from the Main Group of Palau than the Philippine sources. The biggest run-up from the Yap-Palau sources is observed on the east coast of the Ngaraard state – 4.04 m that is bigger than from Philippine1 (3.28 m on the west coast) and Philippine2 (3.7 m on the west coast) sources.

Figure 24. The States of Palau
(picture credits to https://www.mapsofindia.com/world-map/palau/).

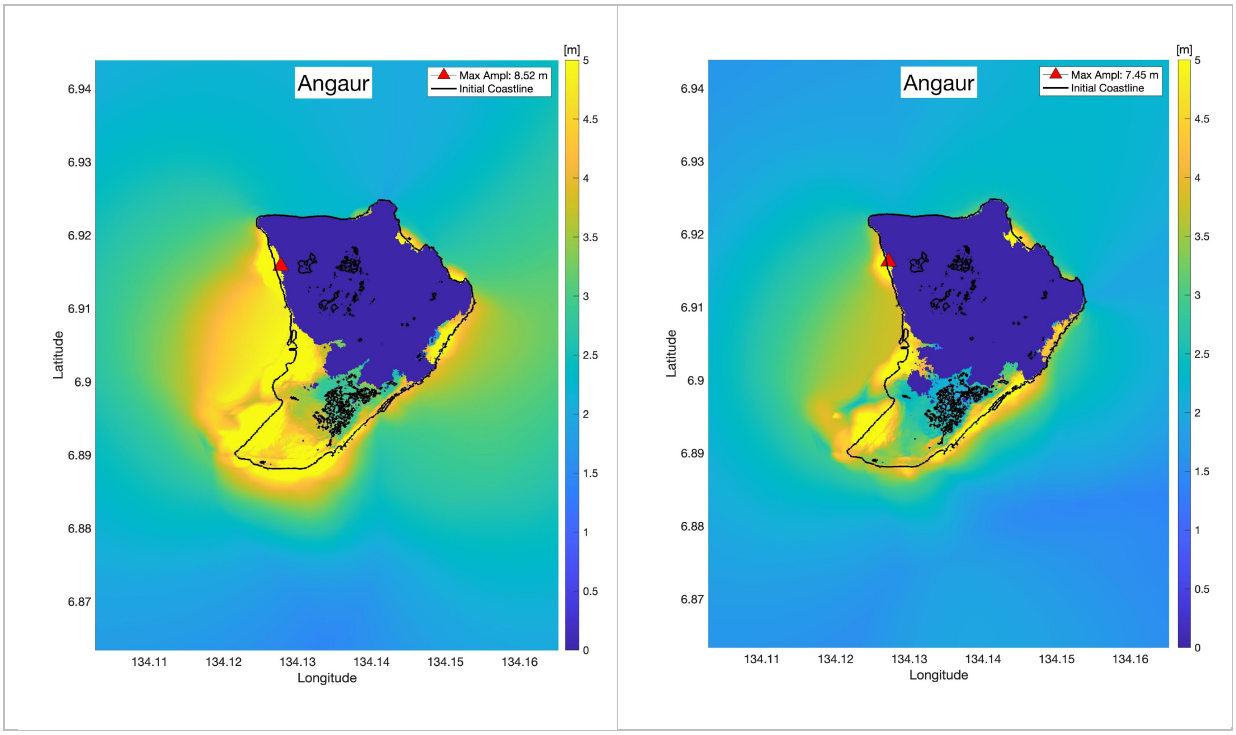
Angaur
Max Ampl: 8.52 m
Initial Coastline
[m]
Latitude
Longitude
6.94
6.93
6.92
6.91
6.9
6.89
6.88
6.87
134.11
134.12
134.13
134.14
134.15
134.16
5
4.5
4
3.5
3
2.5
2
1.5
1
0.5
0
Angaur
Max Ampl: 7.45 m
Initial Coastline
[m]
Latitude
Longitude

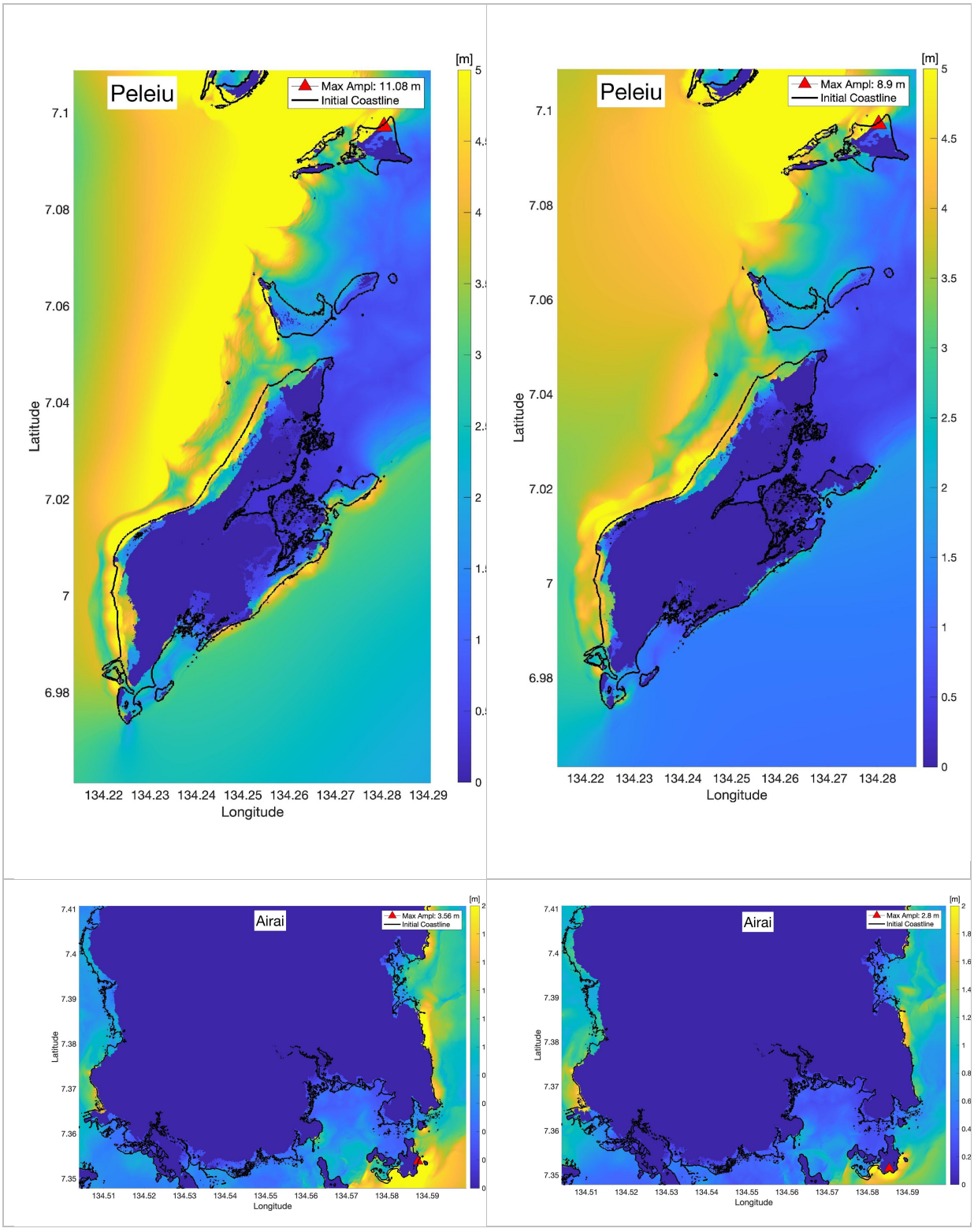
Peleiu
Max Ampl: 11.08 m
Initial Coastline
[m]
Latitude
Longitude
Peleiu
Max Ampl: 8.9 m
Initial Coastline
[m]
Latitude
Longitude
Airai
Max Ampl: 3.56 m
Initial Coastline
[m]
Latitude
Longitude
Airai
Max Ampl: 2.8 m
Initial Coastline
[m]
Latitude
Longitude

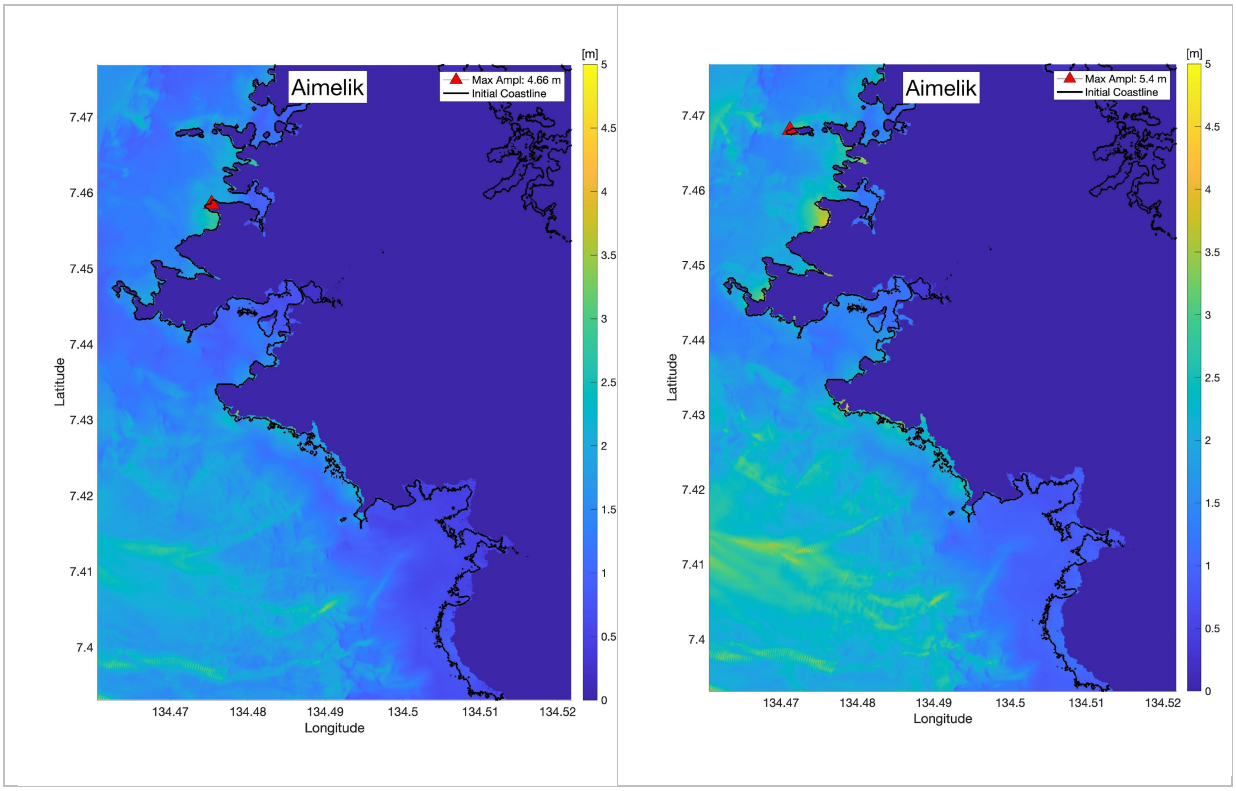
Aimelik
Max Ampl: 4.66 m
Initial Coastline
[m]
Latitude
Longitude
7.47
7.46
7.45
7.44
7.43
7.42
7.41
7.4
134.47
134.48
134.49
134.5
134.51
134.52
Aimelik
Max Ampl: 5.4 m
Initial Coastline
[m]
Latitude
Longitude

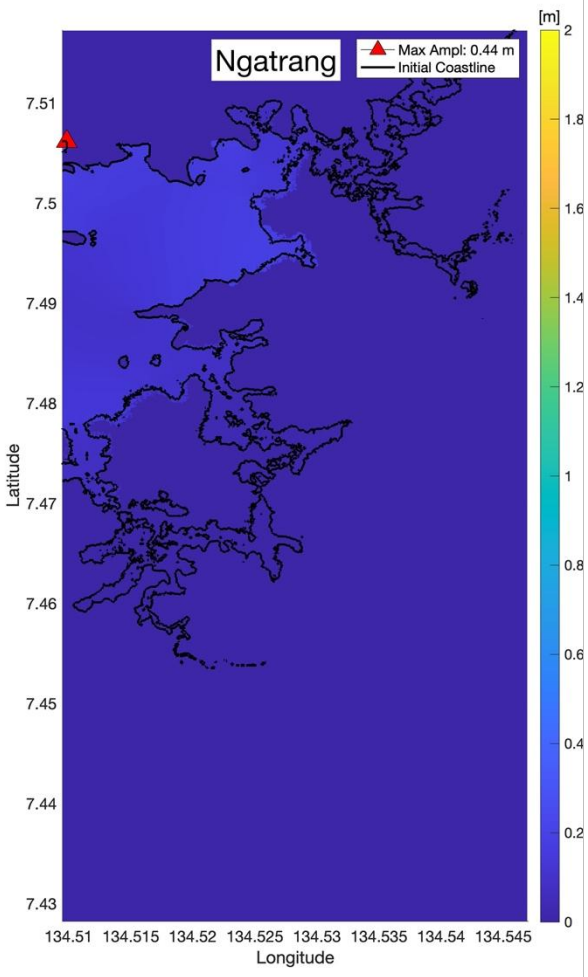
Ngatrang
Max Ampl: 0.44 m
Initial Coastline
[m]
Latitude
Longitude
7.51
7.5
7.49
7.48
7.47
7.46
7.45
7.44
7.43
134.51 134.515 134.52 134.525 134.53 134.535 134.54 134.545

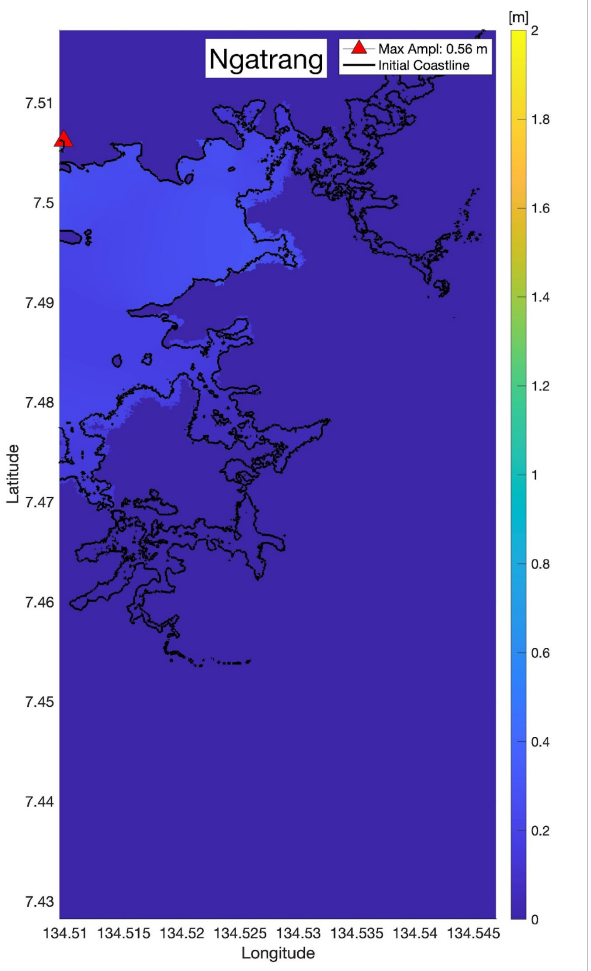
Ngatrang
Max Ampl: 0.56 m
Initial Coastline
[m]
Latitude
Longitude
7.51
7.5
7.49
7.48
7.47
7.46
7.45
7.44
7.43
134.51 134.515 134.52 134.525 134.53 134.535 134.54 134.545

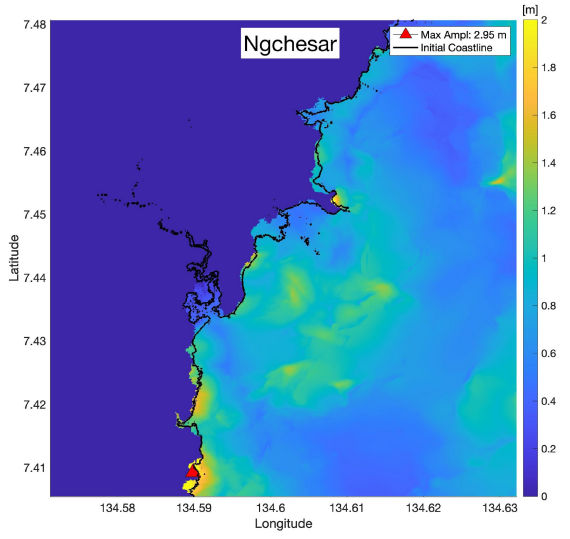
Ngchesar
Max Ampl: 2.95 m
Initial Coastline
[m]
Latitude
Longitude
7.48
7.47
7.46
7.45
7.44
7.43
7.42
7.41
134.58 134.59 134.6 134.61 134.62 134.63

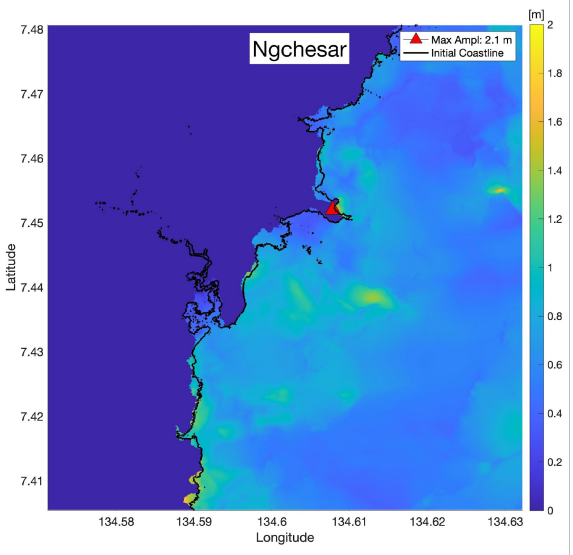
Ngchesar
Max Ampl: 2.1 m
Initial Coastline
[m]
Latitude
Longitude
7.48
7.47
7.46
7.45
7.44
7.43
7.42
7.41
134.58 134.59 134.6 134.61 134.62 134.63

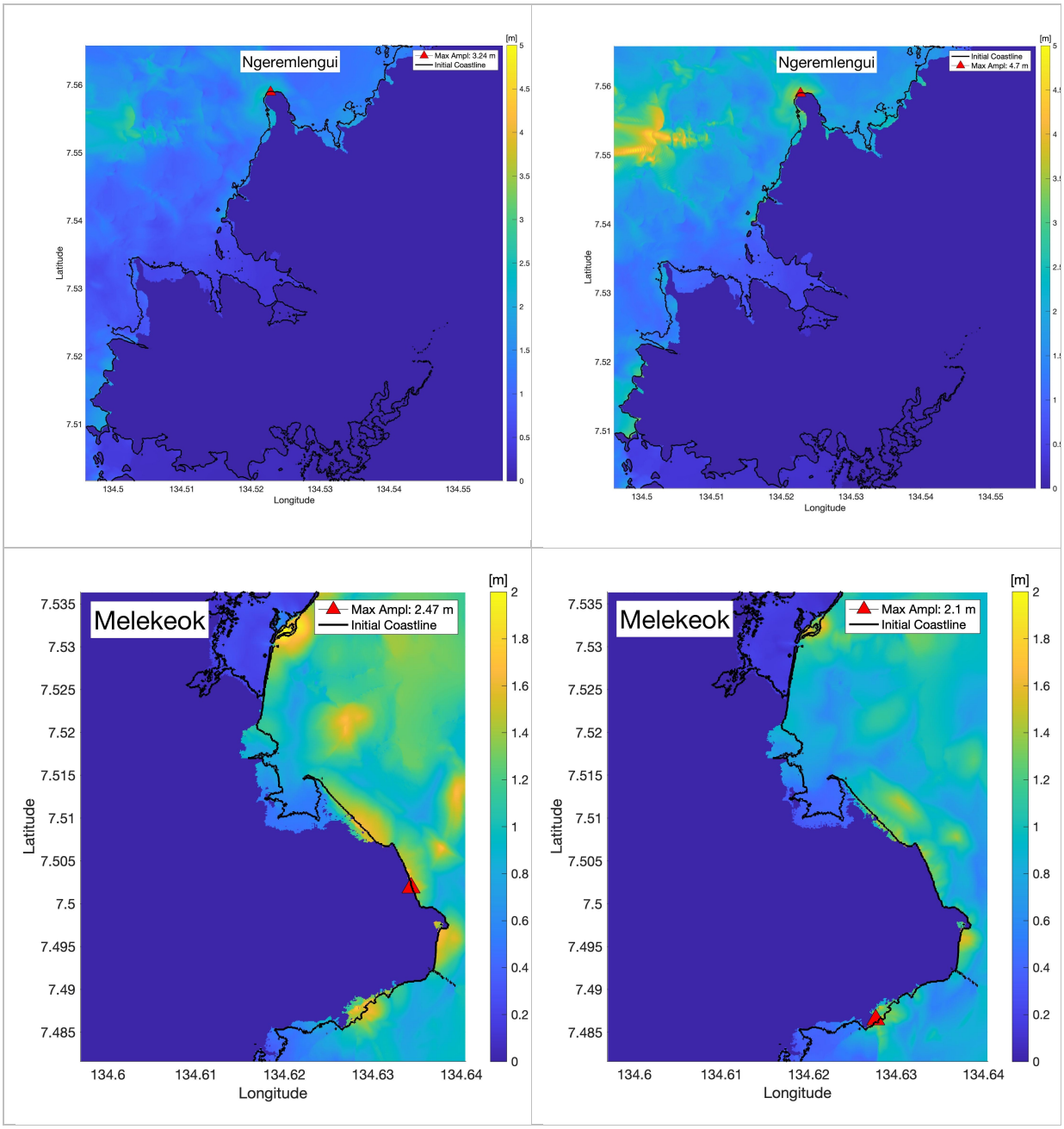
Ngeremlengui
Max Ampl: 3.24 m
Initial Coastline
Ngeremlengui
Initial Coastline
Max Ampl: 4.7 m
Melekeok
Max Ampl: 2.47 m
Initial Coastline
Melekeok
Max Ampl: 2.1 m
Initial Coastline
Latitude
Longitude
[m]

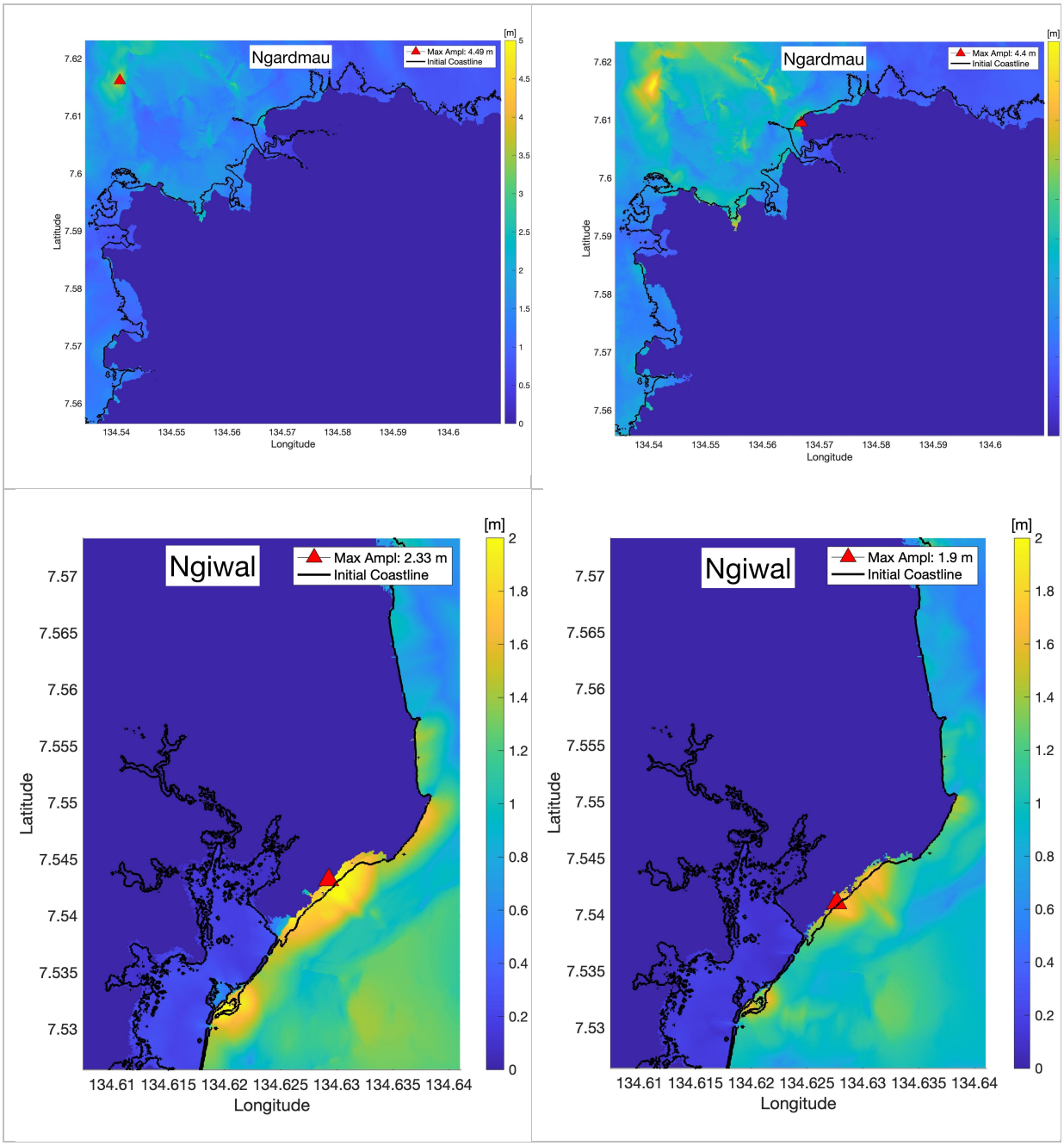
Ngardmau
Max Ampl: 4.49 m
Initial Coastline
[m]
Latitude
Longitude
Ngardmau
Max Ampl: 4.4 m
Initial Coastline
[m]
Latitude
Longitude
Ngiwal
Max Ampl: 2.33 m
Initial Coastline
[m]
Latitude
Longitude
Ngiwal
Max Ampl: 1.9 m
Initial Coastline
[m]
Latitude
Longitude

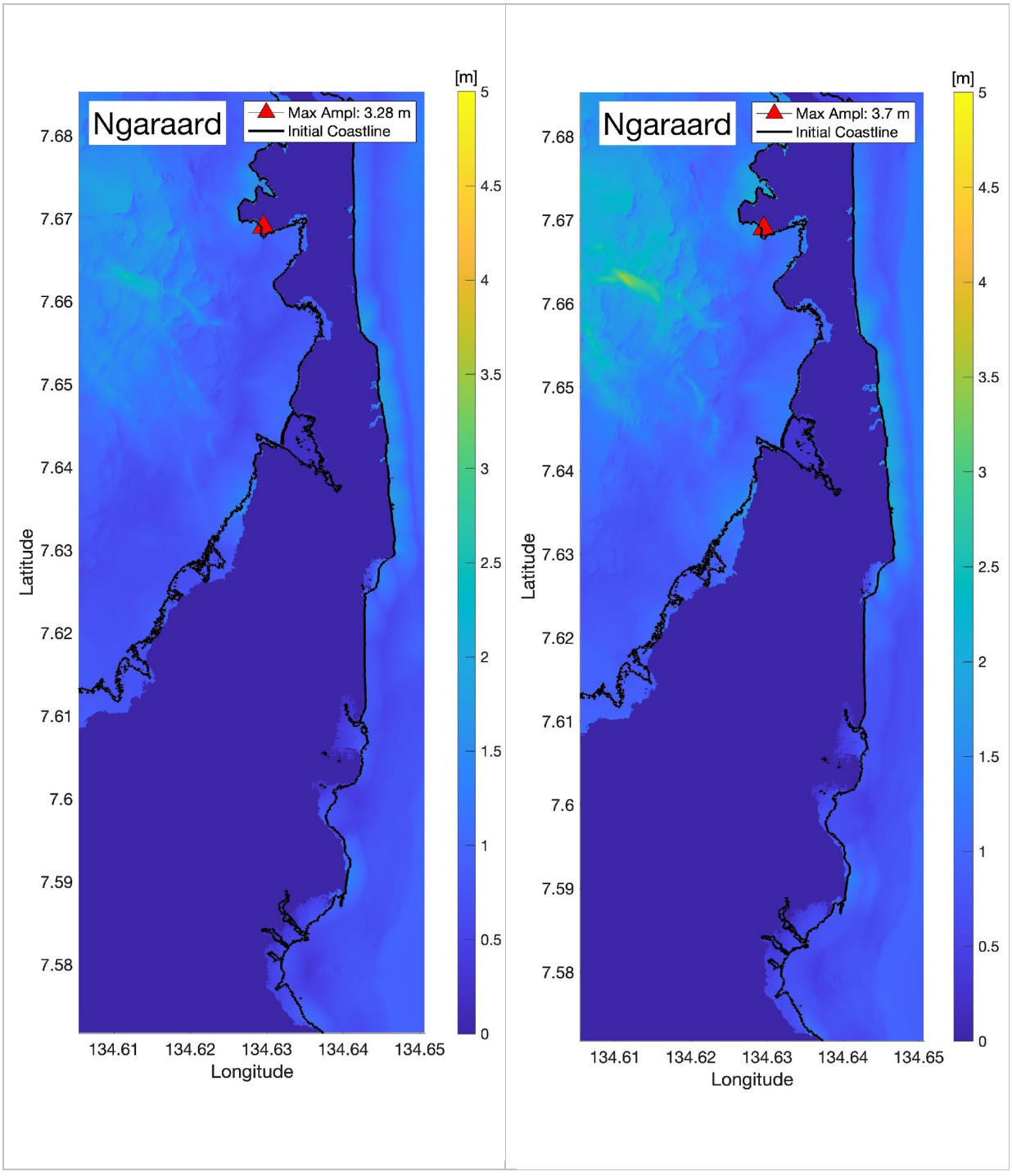
Ngaraard
Max Ampl: 3.28 m
Initial Coastline
[m]
5
4.5
4
3.5
3
2.5
2
1.5
1
0.5
0
7.68
7.67
7.66
7.65
7.64
7.63
7.62
7.61
7.6
7.59
7.58
Latitude
134.61
134.62
134.63
134.64
134.65
Longitude
Ngaraard
Max Ampl: 3.7 m
Initial Coastline
[m]
5
4.5
4
3.5
3
2.5
2
1.5
1
0.5
0
7.68
7.67
7.66
7.65
7.64
7.63
7.62
7.61
7.6
7.59
7.58
Latitude
134.61
134.62
134.63
134.64
134.65
Longitude

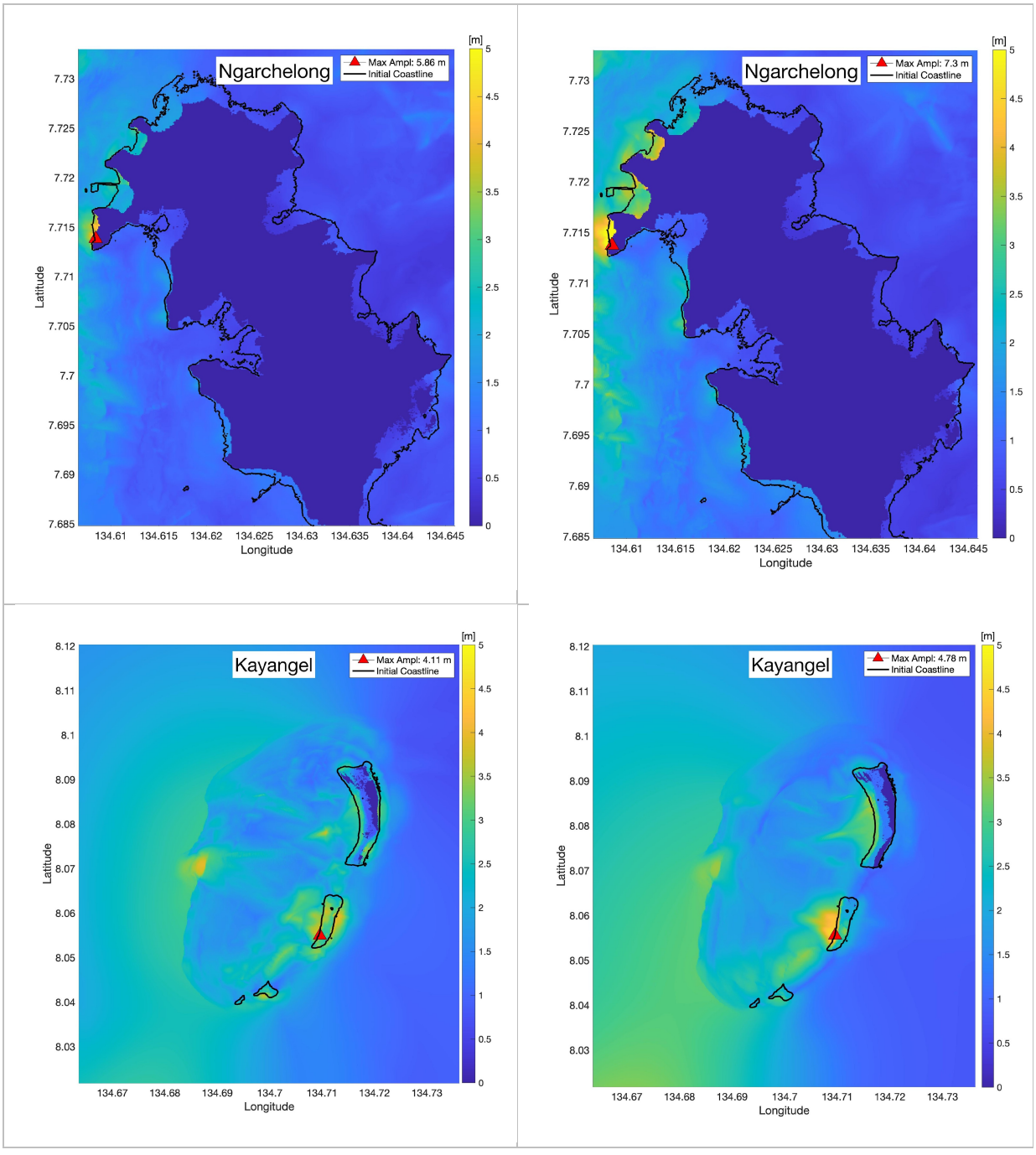

Figure 25. The maximum tsunami height and inundation from the Philippine1 (left column) and Philippine2 (right column) sources. Red triangle marks the position of the overall grid maximum.

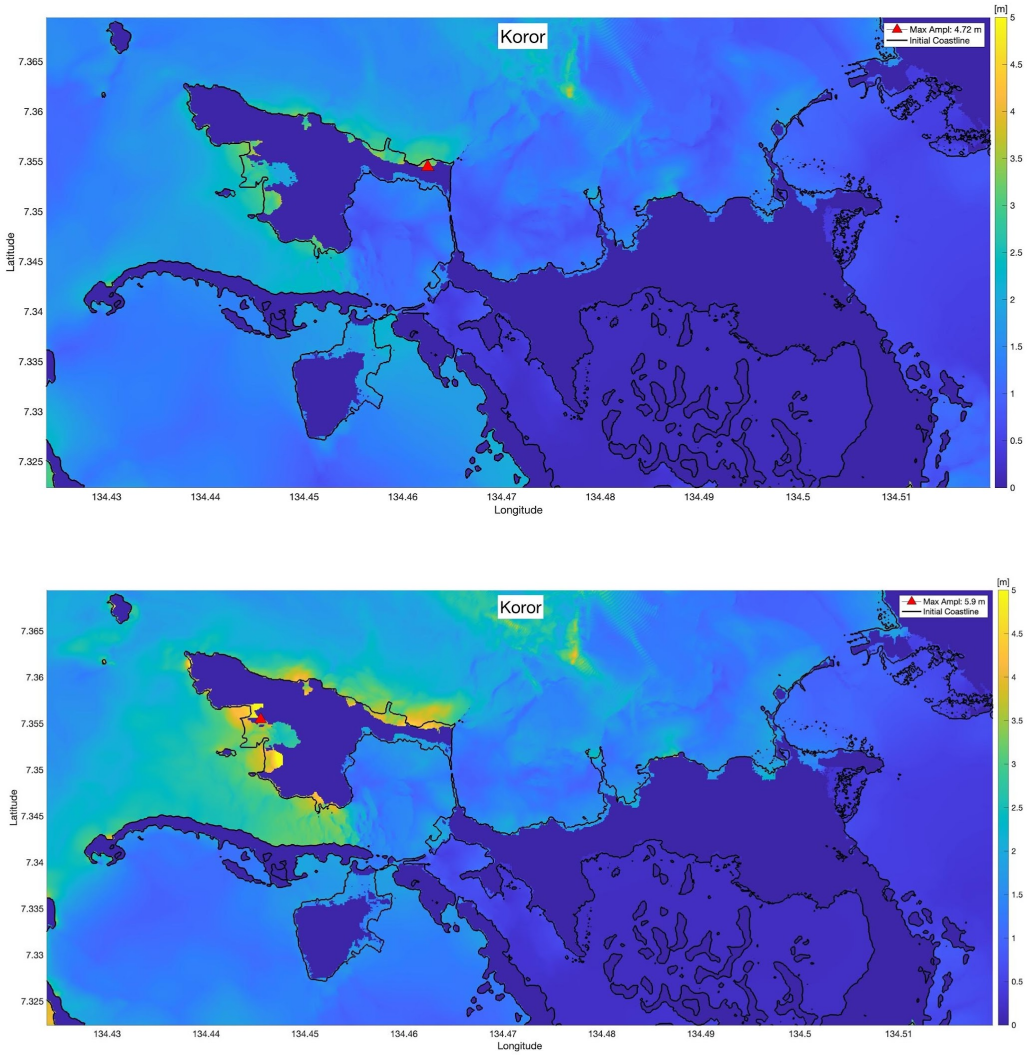

Figure 26. The maximum tsunami height and inundation at Koror from the Philippine1 (*a*) and Philippine2 (*b*) sources. Red triangle marks the position of the overall grid maximum.

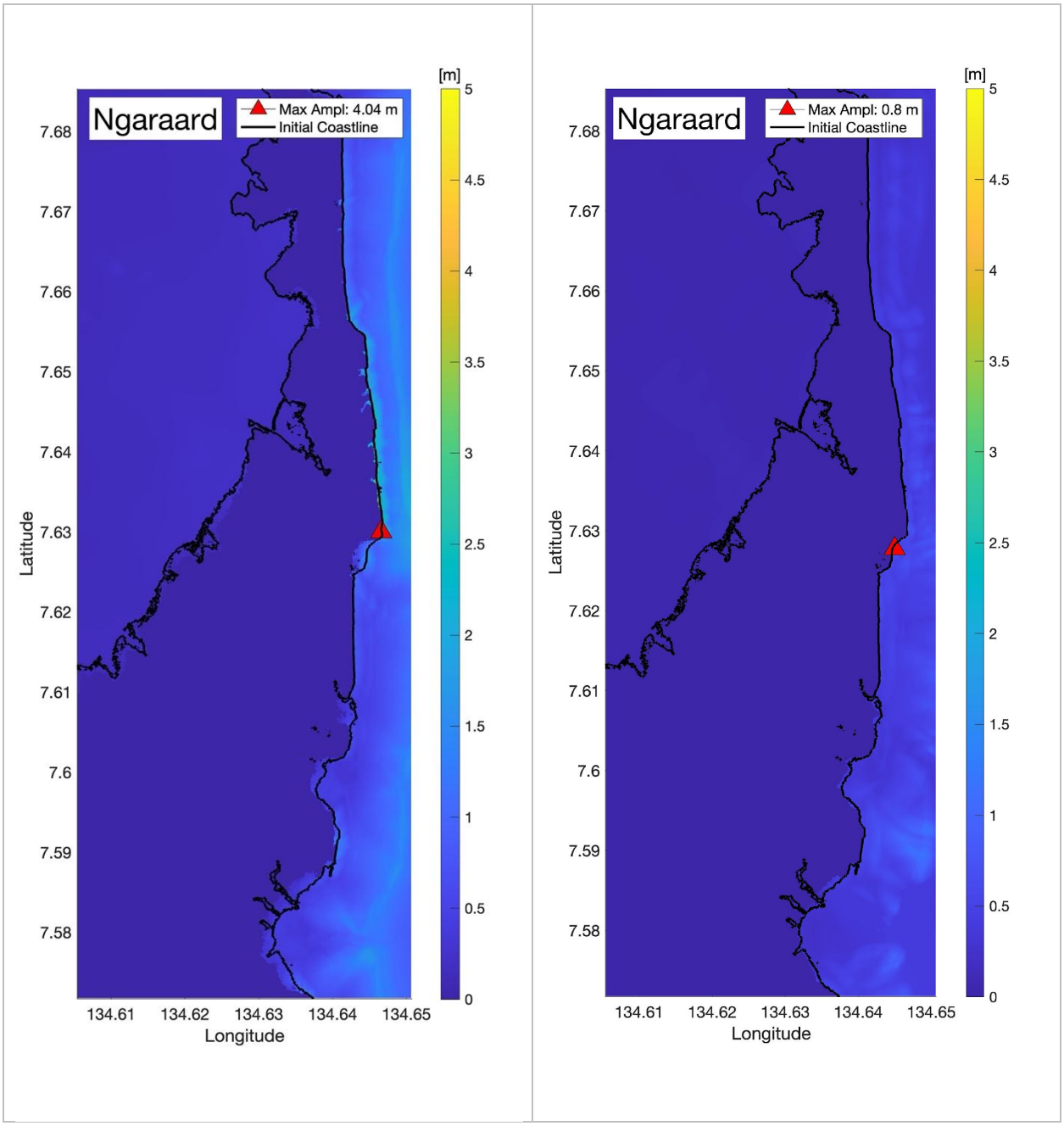
Ngaraard
Max Ampl: 4.04 m
Initial Coastline
[m]
5
4.5
4
3.5
3
2.5
2
1.5
1
0.5
0
7.68
7.67
7.66
7.65
7.64
7.63
7.62
7.61
7.6
7.59
7.58
Latitude
134.61
134.62
134.63
134.64
134.65
Longitude
Ngaraard
Max Ampl: 0.8 m
Initial Coastline
[m]
Latitude
Longitude

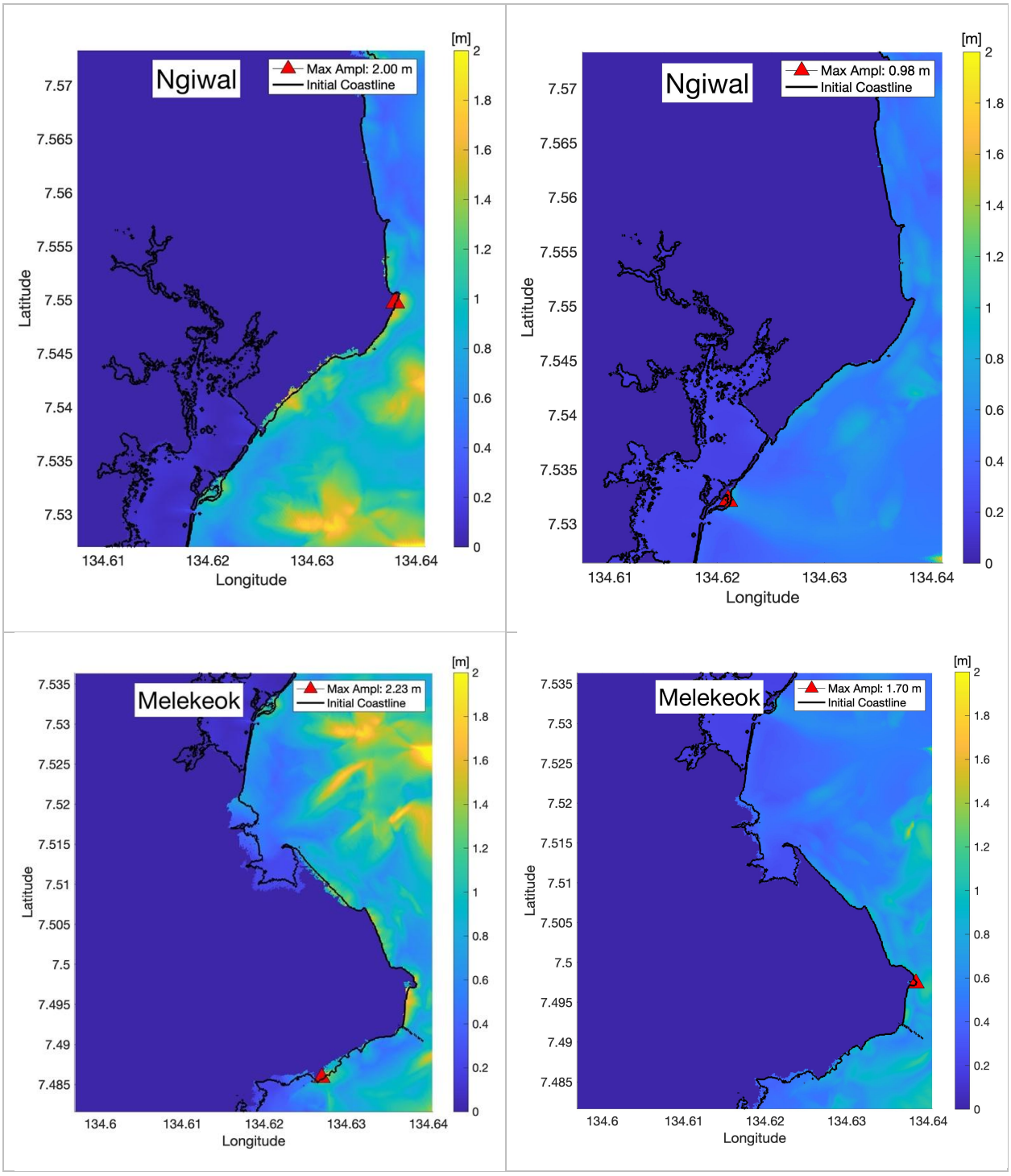
Ngiwal
Max Ampl: 2.00 m
Initial Coastline
Ngiwal
Max Ampl: 0.98 m
Initial Coastline
Melekeok
Max Ampl: 2.23 m
Initial Coastline
Melekeok
Max Ampl: 1.70 m
Initial Coastline
Latitude
Longitude
[m]

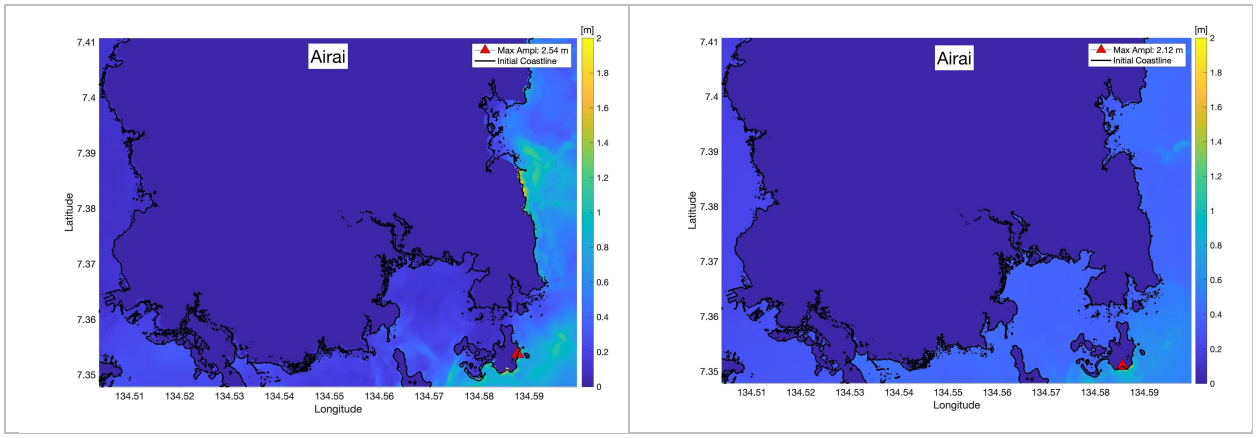

Figure 27. The maximum tsunami height and inundation from the Yap (left column) and Palau (right column) sources. Red triangle marks the position of the overall grid maximum.

The maximum tsunami height plots show the wave pattern, focusing, and run-up elevation. But oftentimes the flow depth is a more intuitive and critical quantity. Flow depth is the wave amplitude minus ground elevation, or the depth of water a person in the flood zone sees. Flow depths greater than .5 m are considered to be dangerous. With this in mind, we provide the highest maximum flow depth for the most hazardous for the Main Palau Group – Philippine1 and Philippine2 sources (Figure 28). The biggest flow depth of 9.25 m is reached in Peleiu state from the Philippine1 source.

Figure 29 shows the maximum flow depth from the Philippine1 (*a*) and Philippine2 (*b*) sources in Koror. There is bigger flow depth on the Ngerekebesang Island from the Philippine2 source and more inundation on Malakal Island from the Philippine1 source. The maximum flow depth is 5.4 m on north-west coast of the Ngerekebesang Island. The background of the figures showing the maximum depth flow is taken from the Open Street Map (OpenStreetMap, 2024). There are differences in the Open Street Map and the modeling DEM coastlines. The Open Street Map uses the MSL vertical datum and the modeling DEM – MHW. We consider the modeling DEM to be more reliable because it is based on very precise LiDAR data.

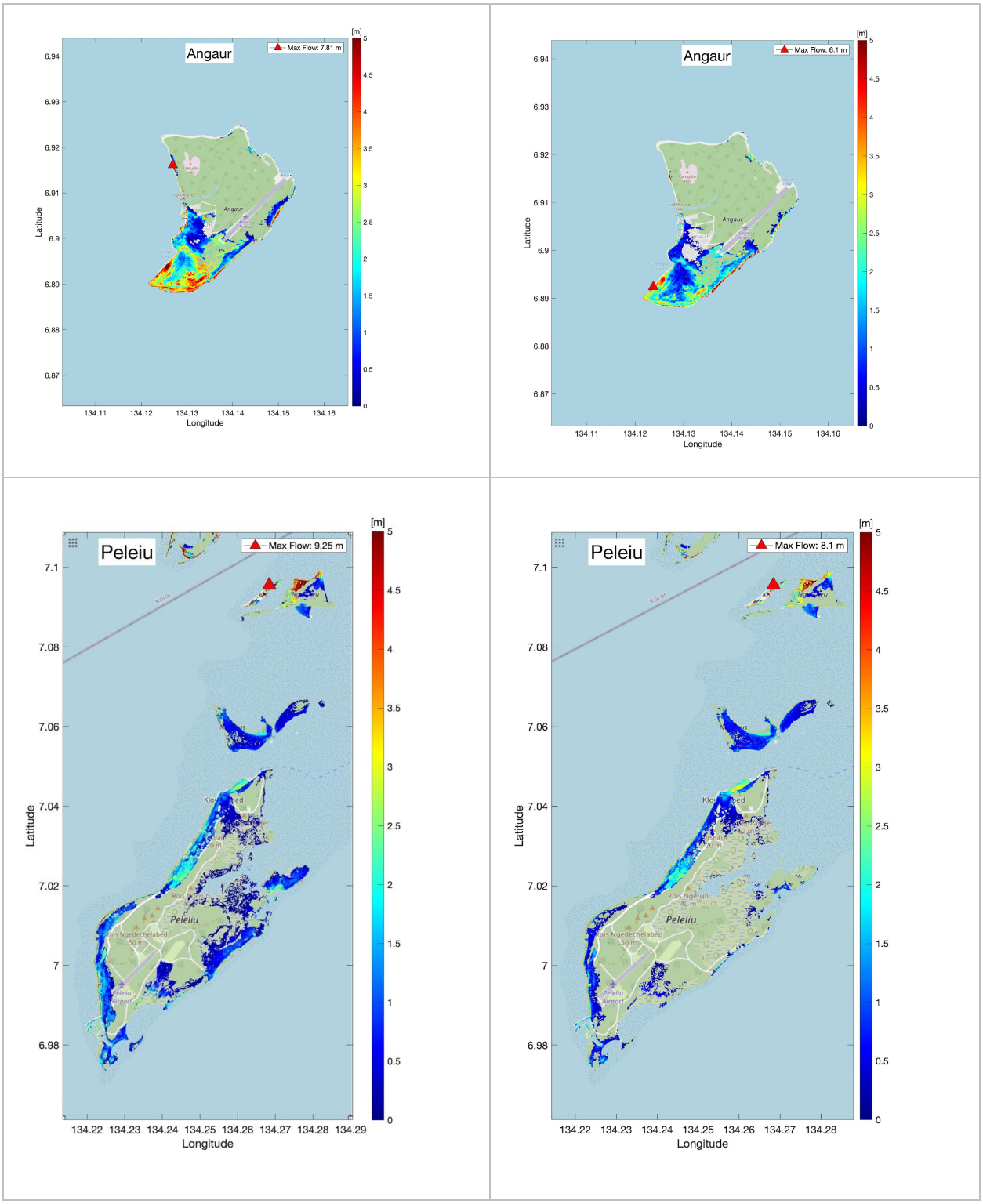

Figure 28. Maximum flow depth from the Philippine1 (left column) and Philippine2 (right column) sources in Peleliu and Angaur states.

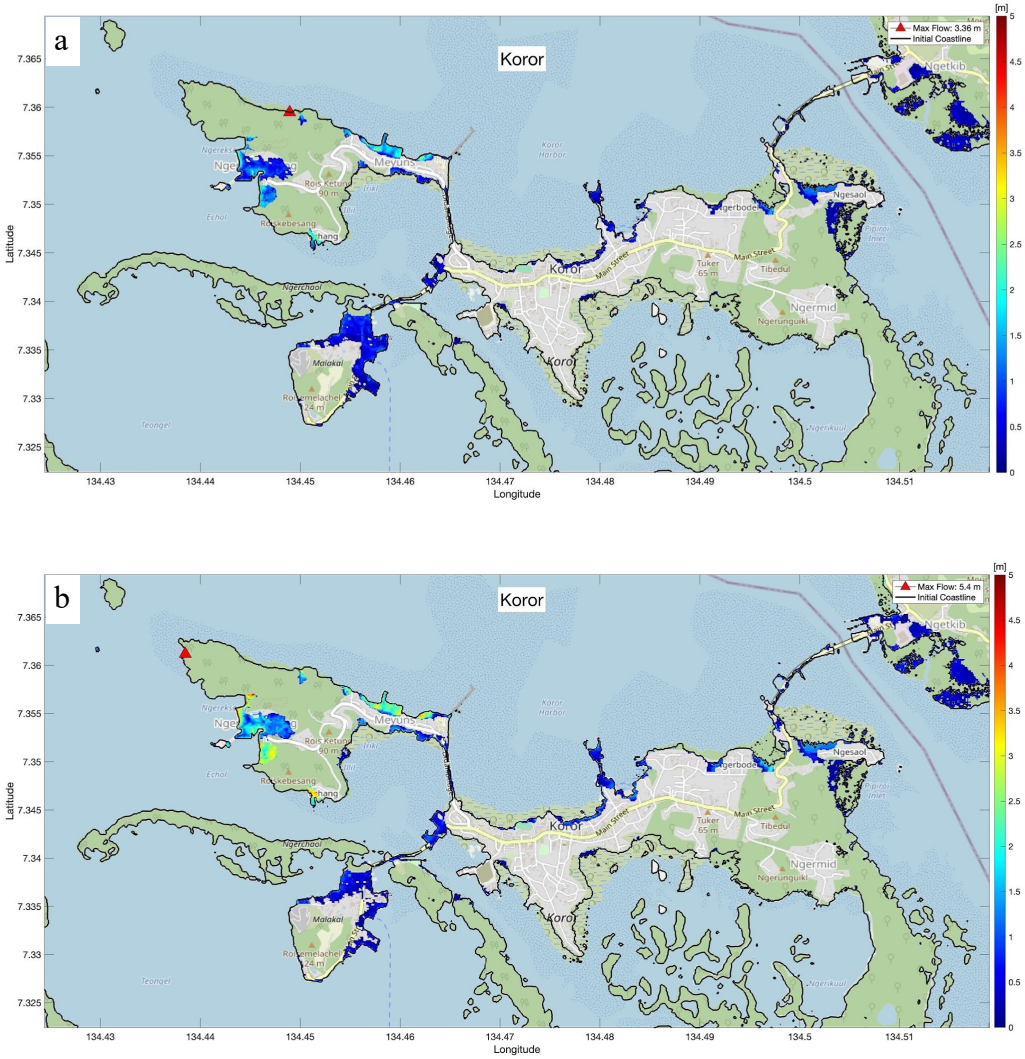

Figure 29. Maximum flow depth from Philippine1 (*a*) and Philippine2 (*b*) sources at Koror.

8.3 Coastal Time Series at Specific Locations

Saving all variables at every time step for the whole simulation is not possible, but the model allows saving chosen locations at every time step and generating a time series. The time series includes the tsunami arrival time, wave amplitude and current speed. For the time series, the tsunami amplitude is the absolute value of the difference between a particular peak or trough of the tsunami and the undisturbed sea level at the time (Figure 30). It is intended to represent the true amplitude of the tsunami wave at some point along the coast. Tsunami heights and current speeds modeled at the dock's locations next to the most populated areas and locations with important infrastructure from the most dangerous for Palau source Philippine2 are presented on Figures 31 and 32.

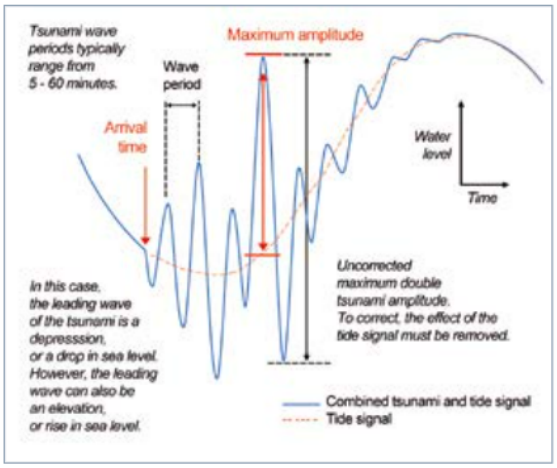

Figure 30. Terms used in the analysis of coastal time series.

Palau coastal wave amplitudes forced by the most hazardous source for Koror vary between -1 to 3.5 meters in the considered coastal locations (Figure 31 and 32). The maximum amplitude exceeds 3.5 meters at #10 – Ngerekebesang Island Echang dock. The wave arrival starts with the rise of water (runup) at the closest to the source and less protected by the reefs locations Peleliu and Angaur 1 hour after the earthquake strikes, and at the furthest locations of the ocean (the east coast of the Babeldaob Island) in 1 hour 15 minutes. The wave reaches the farthest point of the lagoon (#16 Ngerkeseuaol on the Koror Island) in 1 hours 30 minutes. The south coast of Koror is well protected by the set of barrier, fringing, shoreline and lagoon patch reefs and even in the worst-case scenario the amplitudes here do not exceed 40 cm (#16 Ngerkeseuaol, #17 Medalai Land Mark, #18 Medalaii Happy Landing).
Tsunami currents are an obviously important and damaging component of tsunami dynamics, in many cases causing significant hazard to maritime assets. The effects of tsunami currents in nearshore areas have been reported from many locations with docks being destroyed (Dengler, et al., 2008, Wilson, et al., 2013) and large ships breaking free from mooring lines and drifting uncontrolled through their respective ports (Lynett, et al., 2012, Lynett, et al., 2014). Tsunami currents usually accompany large inundations but can happen without them (Lynett, et al., 2014). Therefore, we present here both the time series of wave amplitudes and currents speeds at considered locations.

We highlight here the 3-knot (1.54 meters/second) current speed as the threshold value for currents causing moderate dock/boat damage following tsunami-induced current impacts metrics proposed by Lynett et al., 2014 (Figure 33).

Maximum current speeds and 3-knot current attenuation times (time between wave arrival and when currents drop below 3 knots) are sensitive to the bathymetry, harbor geometry as well as distance to source and source location. Due to the barrier reef bordering the atoll the current speed attenuates on the approach to the coastline especially in the lagoon passes. The maximum current speeds are mostly below 0.5 m/s (0.97 knots) in the well protected by reef areas of the Malakal Harbor at the locations #11, #15 – #18 (Figure 32). Peleliu Kambek (#4) shows the largest consistent currents overall reaching 3.5 m/s (6.8 knots), and the 3-knots attenuation time

of almost 2 hours is the longest of the time series records (Figure 31). The locations #2, #4, #9, #10, #14 reach the 3-knots current attenuation.

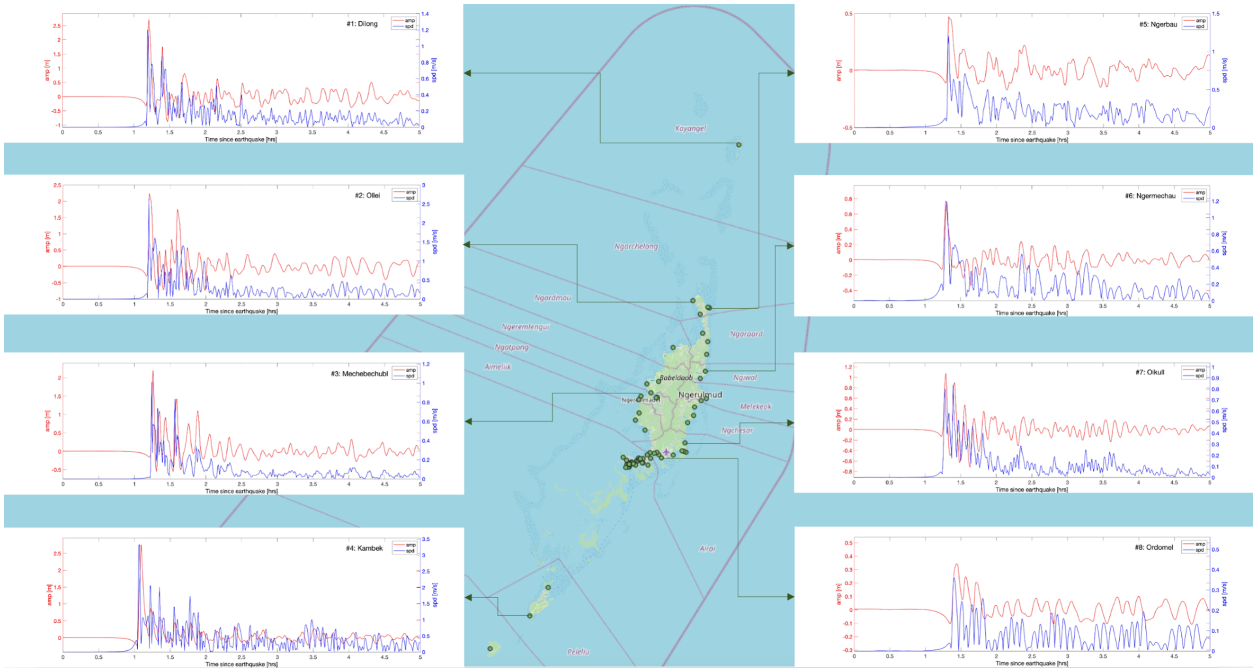

Figure 31. Time series of wave amplitude (red) and current speed (blue) from the Philippine2 source at eight dock's location around the Main Group of Palau.

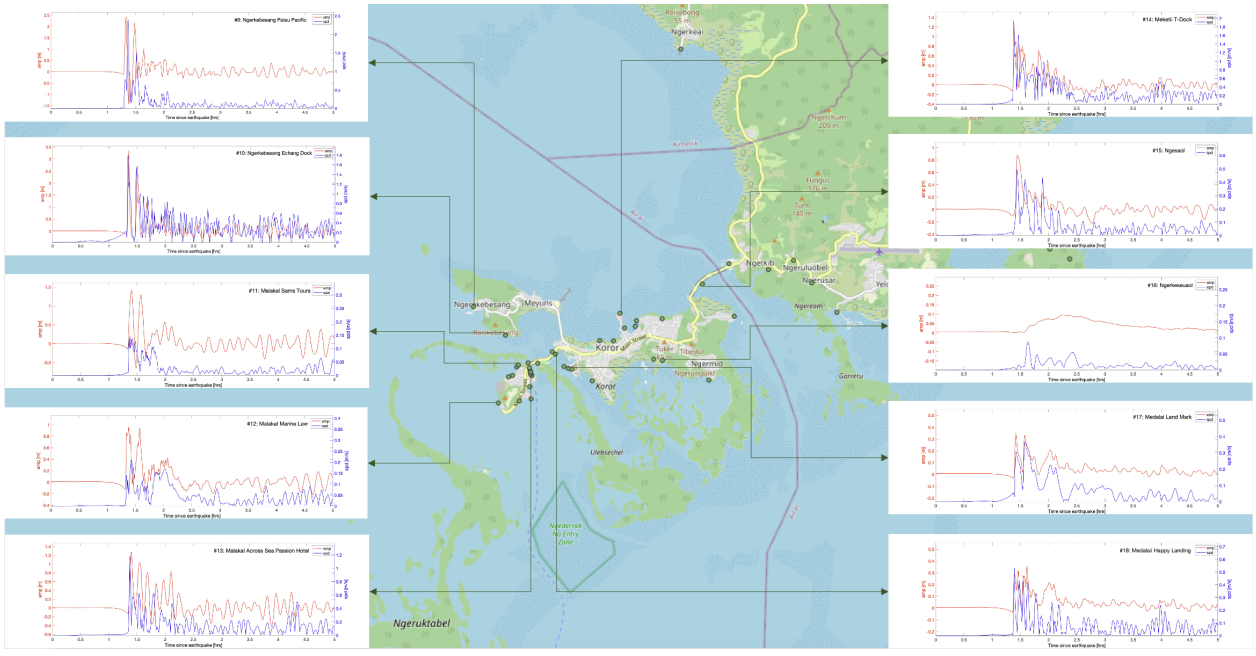

Figure 32. Time series of wave amplitude (red) and current speed (blue) from the Philippine2 source at ten dock's location around the Koror State of Palau.

Damage Index	Damage Type
5	Complete destruction
4	Major dock/boat damage, large vessels off moorings
3	Moderate dock/boat damage, mid-sized vessels off moorings
2	1-2 docks/small boats damaged, large buoys moved
1	Small buoys moved
0	No damage

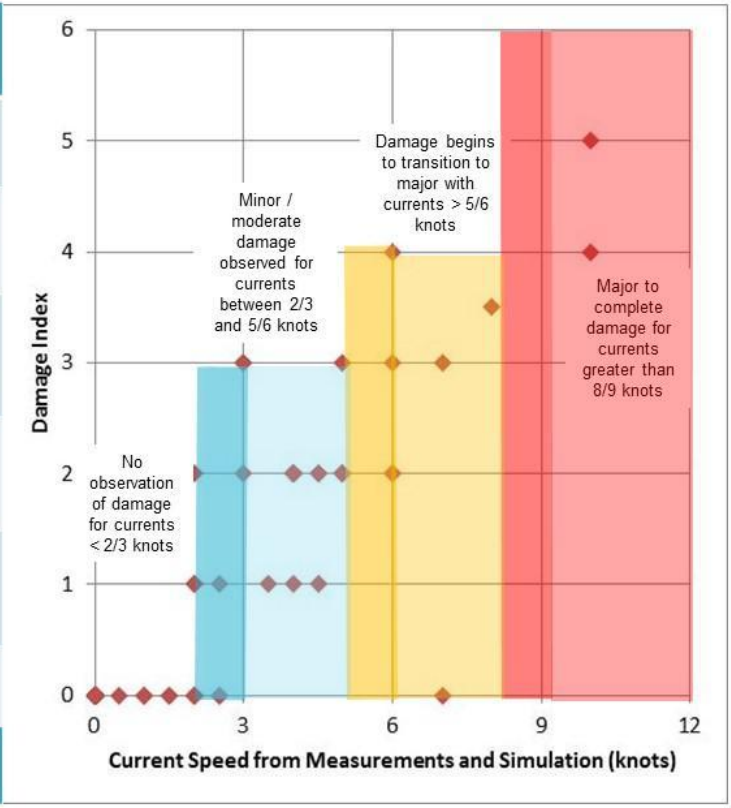

Figure 33. Scatter plot of observed damage indices and their corresponding tsunami-induced current with potential damage description (https://calema.maps.arcgis.com/apps/MapSeries/index.html?appid=baea43e6453b49ff9ae3f967eb6935be modified from Lynett et al., 2014).

8.4 Maximum Currents and Duration

In this section we provide overall maximum current speed and duration information as two-dimensional map plots. Maximum current plots are shown at Figure 34 as a color-filled contours binning current speed into four bins: 0-3 knots (blue), 3-6 knots (cyan), 6-9 knots (yellow) and above 9 knots (red), as recommended by the proceedings of the NTHP Tsunami Current Modeling Workshop (NTHMP, 2017).

The maximum currents occur in areas where a constriction occurs: between reefs, islands or at the mouth of a bay, but the attenuation time (time it takes for currents to fall below the 3-knot cutoff) depends on many factors including harbor resonance.

The outer reef serves as a barrier to the approaching tsunami: part of the wave reflects from the fore reef, the rest of it slows down while moving along the reef flat toward the shore. This behavior can be seen well at the west part of the atoll (Figure 34). The maximum currents are getting bigger in passes between the reefs and in bays formed by the reefs exceeding the 9-knot threshold in Toachel Mlengui (West Passage) and Aiwokako Passage.

The 3-knot current attenuation times are the longest along the outer part of the west barrier reefs, exceeding at some areas 3 hours (Figure 35).

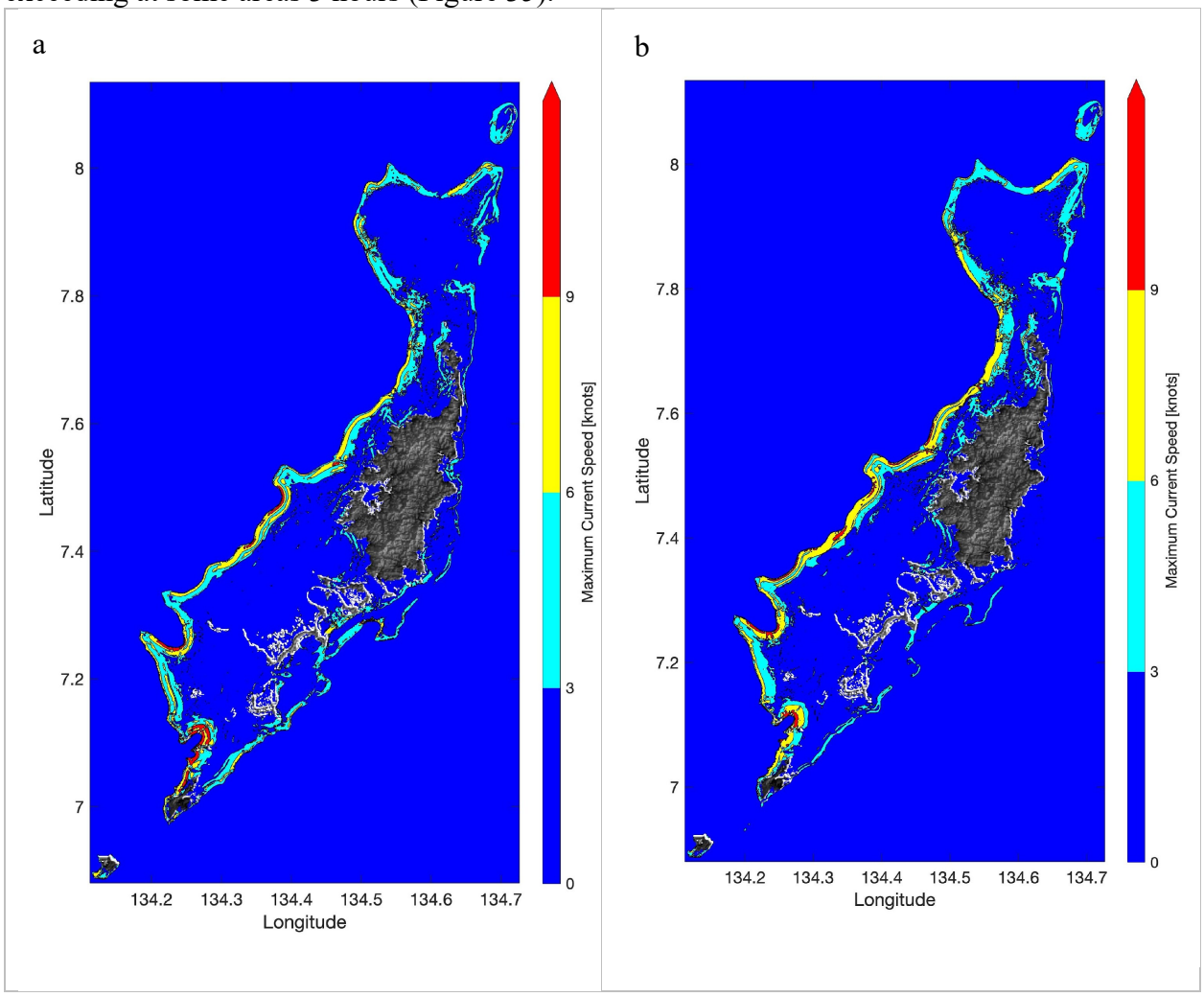

Figure 34. Maximum current speeds in Palau from the Phillipine1 (*a*) and the Philippine2 (*b*) sources.

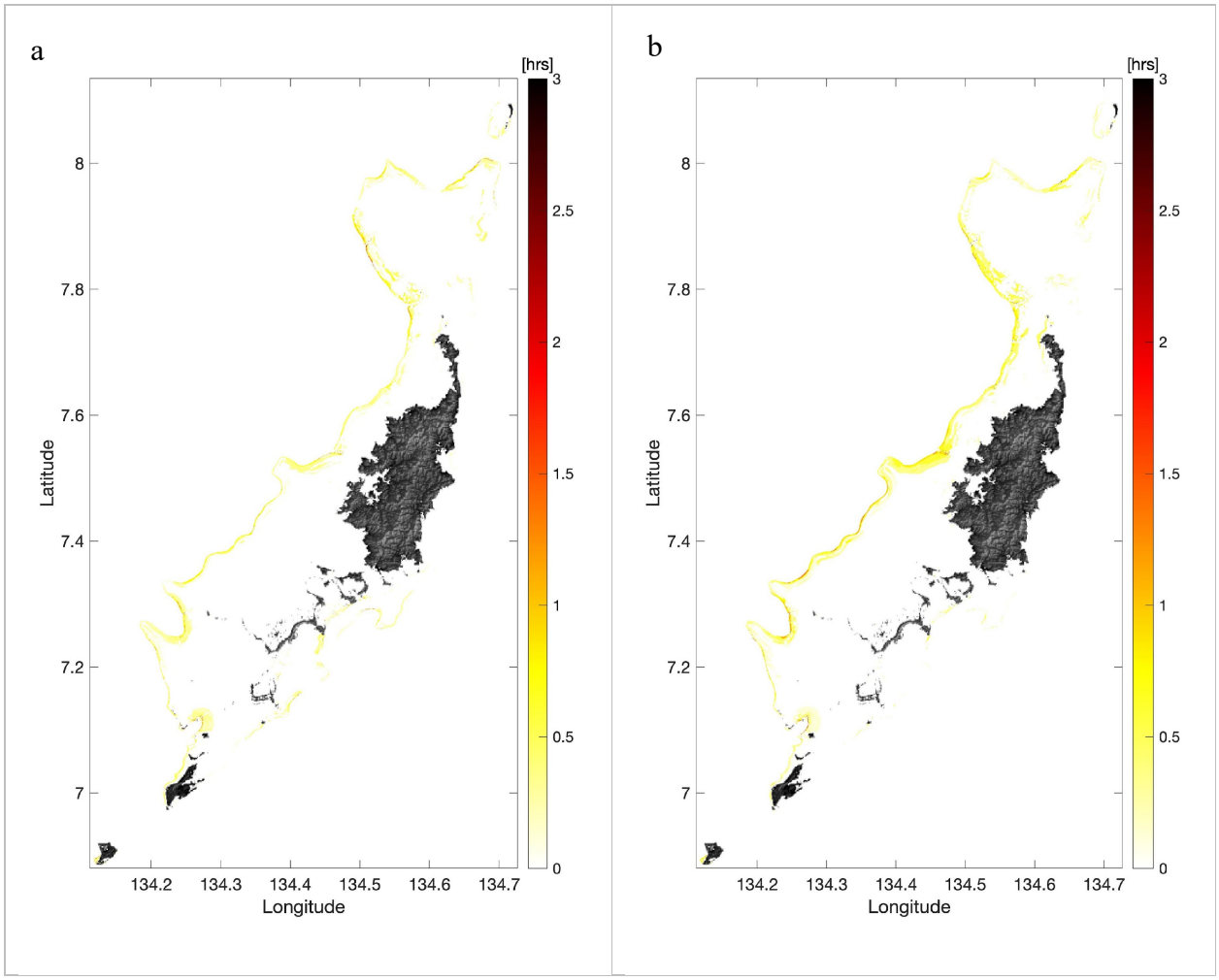

Figure 35. 3-knot current attenuation time in Palau from the Phillipine1 (*a*) and the Philippine2 (*b*) sources.

8.5 Composite Results

This project has identified two sources with potential significant impact on Palau, and has focused so far on the most hazardous as they provide the largest inundation. But it is possible that smaller events inundate an area that a larger source has not, either because the incident direction of wave fronts from the two sources come from different directions, or because the dynamics of the wave as it shoals causes a focusing specific to a certain source. For this reason, we create a composite maximum by taking the envelope of maximum output from each source (e.g., the maximum of the maximums) (Figure 36 and 37). This composite maximum amplitude and depth flow looks very much like the combination of two from the most hazardous source Philippines1 and Philippines2 (Figure 26 and 29) shown in section 8.2. For example, the tsunami originated from the Philipine1 source causes the bigger inundation in Malakal Island and the tsunami from the Philipine2 source has the higher run-ups at Ngerekebesang Island.

Patterns for Palau inundation are typical for those seen in most islands: low-lying beach areas experience the worst inundation, coral reefs serve as a protecting barrier from tsunami and tend to mitigate inundation, significantly reduce the velocity of a wave approaching the shore and in general lower the potential tsunami impact.

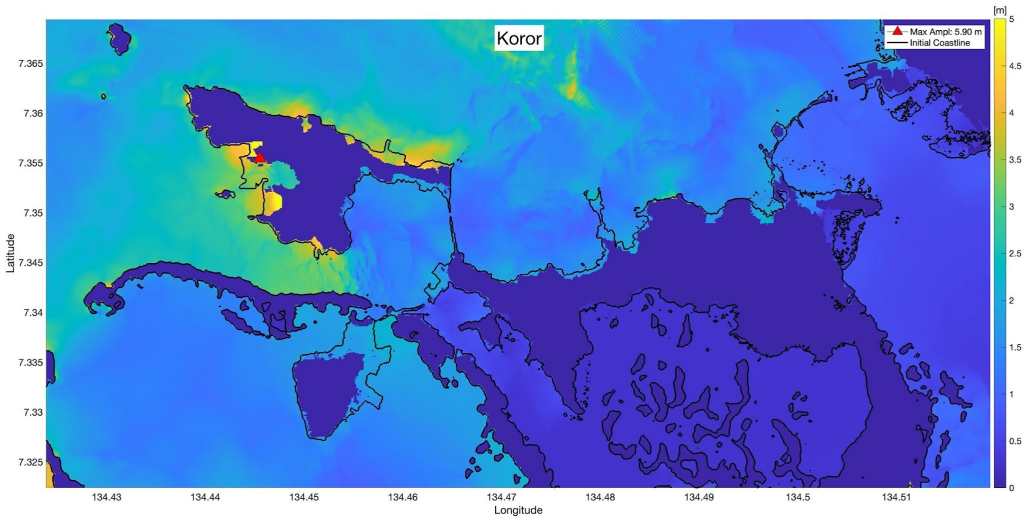

Figure 36. Composite maximum tsunami height at Koror.

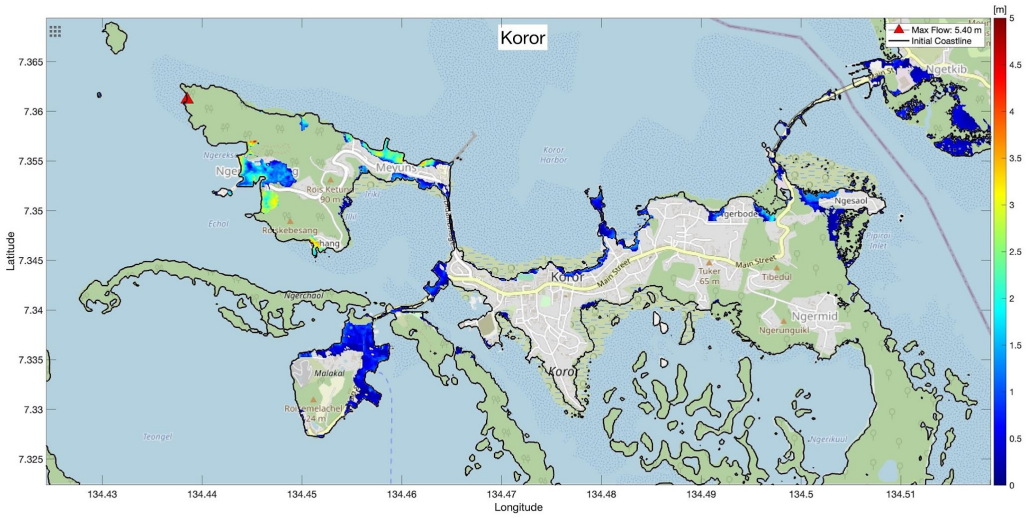

Figure 37. Composite maximum tsunami flow depth at Koror.

9. Conclusion

The aim of this project was to do a thorough scenario-based tsunami inundation study using the worst-case scenarios to identify the possible tsunami impact to the Main Palau Group. The Republic of Palau is surrounded by the Pacific Ocean "Ring of Fire" – extremely active seismic zones, which align with the boundaries of the tectonic plates. The sensitivity study using the NOAA Tsunami Forecast Propagation Database conducted to model tsunami impact along the coastline of Palau from tsunami originating from 138 discrete earthquake sources located all around the Pacific helped to identify two the most potentially hazardous sources from Philippine

Trench and two additional closest to Palau sources with the significant impact (one source from Palau and one from Yap Trenches). Arrival times for waves from the most hazardous source range from 1 hour at Angaur and Peleiu to 1 hour 30 minutes at lagoon on the south from Koror. The overall maximum tsunami height of 11.08 m reached north of Carp Island at Peleiu State. The biggest tsunami run-ups with extensive inundations are observed in Angaur and Peleiu states due to the shorter distance to the source and lesser reef protection than other states.

The outer reef serves as a barrier to the approaching tsunami: part of the wave reflects from the fore reef, the rest of it slows down while moving along the reef flat toward the shore. The maximum currents are getting bigger in passes between the reefs and in bays formed by the reefs exceeding the 9-knot threshold in Toachel Mlengui (West Passage) and Aiwokako Passage.

The 3-knot current attenuation times are the longest along the outer part of the west barrier reefs, exceeding at some areas 2 hours.

The composite maximum amplitude and depth flow look very much like the combination of two from the most hazardous source.

Patterns for Palau inundation are typical for those seen in most islands: low-lying beach areas experience the worst inundation, coral reefs serve as a protecting barrier from tsunami and tend to mitigate inundation, significantly reduce the velocity of a wave approaching the shore and in general lower the potential tsunami impact.

This study provides a good first step toward assessing the effect of tsunamigenic earthquakes on Palau. However, this study does not consider tsunami generating volcanic eruptions and tsunamigenic landslides that may occur due to earthquakes or volcanic activity.

Model output products are provided (in GIS-readable TIFF format). They include the composite maximum tsunami amplitudes and the maximum flow depths over all sources.

REFERENCES

U.S. Census Bureau. 2020 Census Results. Washington, DC: U.S. Department of Commerce, 2021. https://www.census.gov/programs-surveys/decennial-census/decade/2020/2020-census-results.html.

NTHMP, 2017, Proceedings and Results of the National Tsunami Hazard Mitigation Program 2015 Tsunami Current Modeling Workshop, February 9 – 10, 2015, Portland, Oregon: compiled by Patrick Lynett and Rick Wilson, 194 p.

OpenStreetMap contributors. (2024). *OpenStreetMap*. Retrieved September 13, 2024, from https://www.openstreetmap.org

NOAA National Centers for Environmental Information (NCEI), 2024, National Geophysical Data Center / World Data Service: NCEI/WDS Global Historical Tsunami Database. https://doi.org/10.7289/V5PN93H7

Zhang W, Qi J, Wan P, Wang H, Xie D, Wang X, Yan G. An Easy-to-Use Airborne LiDAR Data Filtering Method Based on Cloth Simulation. Remote Sensing. 2016; 8(6):501.

University of Hawaii Sea Level Center. (2024). Tide gauge data: Malakal, Palau. UHSLC. https://uhslc.soest.hawaii.edu/stations/?stn=007#datums

National Geospatial-Intelligence Agency. (2024). *Nautical chart:* [81145 PALAU ISLANDS (Northern Part)]. NGA. https://msi.nga.mil/Products

National Geospatial-Intelligence Agency. (2024). *Nautical chart:* [81141 PALAU ISLANDS]. NGA. https://msi.nga.mil/Products

National Geospatial-Intelligence Agency. (2024). Nautical chart: [81148 Toachel Mlengui (West Passage) (PALAU ISLANDS)]. NGA. https://msi.nga.mil/Products

National Geospatial-Intelligence Agency. (2024). *Nautical chart:* [81151 ARANGEL CHANNEL AND KOROR ROAD (PALAU ISLANDS)]. NGA. https://msi.nga.mil/Products

National Geospatial-Intelligence Agency. (2024). *Nautical chart:* [81155 MALAKAL HARBOR (PALAU ISLANDS)]. NGA. https://msi.nga.mil/Products

National Oceanic and Atmospheric Administration. (2024). Nautical chart [US3PLW01]. U.S. Department of Commerce, Office of Coast Survey. https://charts.noaa.gov/InteractiveCatalog/nrnc.shtml

National Oceanic and Atmospheric Administration. (2024). Nautical chart [US456660]. U.S. Department of Commerce, Office of Coast Survey. https://charts.noaa.gov/InteractiveCatalog/nrnc.shtml

National Oceanic and Atmospheric Administration. (2024). Nautical chart [US556660]. U.S. Department of Commerce, Office of Coast
Survey. https://charts.noaa.gov/InteractiveCatalog/nrnc.shtml

National Oceanic and Atmospheric Administration. (2024). Nautical chart [US456662]. U.S. Department of Commerce, Office of Coast
Survey. https://charts.noaa.gov/InteractiveCatalog/nrnc.shtml

NOAA National Centers for Environmental Information (NCEI). (2024). Gridded multibeam bathymetric data from surveys archived at NOAA's National Centers for Environmental Information (NCEI). [Bathymetry Data]. https://www.ncei.noaa.gov/maps/bathymetry/

Ryan, W.B.F., Carbotte, S.M., Coplan, J.O., O'Hara, S., Melkonian, A., Arko, R., Weissel, R.A., Ferrini, V., Goodwillie, A., Nitsche, F., Bonczkowski, J., and Zemsky, R. (2009). Global Multi-Resolution Topography (GMRT) Synthesis Version 3.9. Integrated Earth Data Applications (IEDA). https://doi.org/10.1594/IEDA.000001

Bird, P., 2003, An updated digital model of plate boundaries, *Geochem. Geophys. Geosys.*, 4(3): 1027. doi:10.1029/2001GC000252.

Rong, Y., J. Park, D. Duggan, M. Mahdyiar and P. Bazzurro, 2016, Probabilistic seismic hazard assessment for Pacific Island countries, In: Rock Anisotropy, Fracture and Earthquake Assessment, pp. 264 – 282. https://doi.org/10.1515/9783110432510-007

Synolakis, C.E., E.N. Bernard, V.V. Titov, U. Kânoğlu, F.I. González, 2008, Validation and verification of tsunami numerical models, *Pure Appl. Geophys.*, 165 (11 – 12), pp. 2197 – 2228. https://doi.org/10.1007/s00024-004-0427-y

Moore, C., and Arcas, D., 2019, Modeling tsunami inundation for hazard assessment of the U.S. Virgin Islands, *NOAA Technical Memorandum*, 37 p.

Schäfer, A. M., & Wenzel, F. (2019). Global megathrust earthquake hazard—Maximum magnitude assessment using multi-variate machine learning. *Frontiers in Earth Science*, *7:136*, 1-19. https://doi.org/10.3389/feart.2019.00136

Rong, Y., Jackson, D. D., Magistrale, H., and Goldfinger, C. (2014). Magnitude limits of subduction zone earthquakes. *Bull. Seismol. Soc. Am. 104*, 2359–2377. https://doi.org/10.1785/0120130287

McCaffrey, R. (2008). Global frequency of magnitude 9 earthquakes. *Geology 36*, 263–266. https://doi.org/10.1130/G24402A.1

Berryman, K.,Wallace, L., Hayes, G., Bird, P.,Wang, K., Basili, R., et al. (2015). The GEM Faulted Earth Subduction Interface Characterisation Project, Version 2.0, April 2015. Available

online at: https://issuu.com/gem_wrld/docs/gem-gc-fe-gem_faulted_earth_project (accessed September 16, 2024).

Davies, G., Griffin, J., Løvholt, F., Glimsdal, S.,Harbitz, C., Thio, H. K., et al. (2017). A global probabilistic tsunami hazard assessment from earthquake sources. *Geol. Soc. Lond. Spec. Publicat. 456, SP456–5*. https://doi.org/10.1144/SP456.5

Løvholt, F., Glimsdal, S., Harbitz, C.B., Zamora, N., Nadim, F., Peduzzi, P., Dao, H.I., Smebye, H., 2011, Tsunami hazard and exposure on the global scale, *Earth-Science Reviews*, 0012-8252. https://doi.org/10.1016/j.earscirev.2011.10.002

Gica, E., M.C. Spillane, V.V. Titov, C.D. Chamberlin, and J.C. Newman, 2008, Development of the forecast propagation database for NOAA's Short-term Inundation Forecast for Tsunamis (SIFT), *NOAA Tech. Memo*., OAR PMEL-139, NOAA/Pacific Marine Environmental Laboratory, Seattle, WA, 89 p.

Uslu, B., 2009, Deterministic and probabilistic tsunami studies in California from near and far-field sources, Ph.D. thesis, University of Southern California, Los Angeles, California, 161 p.

Dengler, L.A., Uslu, B., Barberopoulou, A., Borrero, J.C., Synolakis, C., 2008, The vulnerability of Crescent City, California, to tsunamis generated by earthquakes in the Kuril Islands region of the northwestern Pacific, *Seismol. Res. Lett.*, 79 (5), 608 – 619. https://doi.org/10.1785/gssrl.79.5.608

GEBCO Compilation Group, 2021, GEBCO 2021 Grid. https://doi.org/10.5285/c6612cbe-50b3-0cff-e053-6c86abc09f8f

Liu, P.L.-F., Cho, Y.S., Briggs, M.J., Kânoğlu, U., Synolakis, C.E., 1995, Runup of solitary waves on a circular island, *Journal of Fluid Mechanics*, 302, pp. 259 – 285. https://doi.org/10.1017/S0022112095004095

Briggs, M.J., Synolakis, C.E., Harkins, G.S., Green, D.R., 1995, Laboratory experiments of tsunami runup on a circular island, *Pure and Applied Geophysics*, 144 (3 – 4), pp. 569 – 593. https://doi.org/10.1007/978-3-0348-7279-9_12

Kânoğlu, U., 1998, The runup of long waves around piecewise linear bathymetries, Ph.D. thesis, University of Southern California, Los Angeles, California, 292 p. https://doi.org/10.25549/usctheses-c17-385538

Wells, D. L., & Coppersmith, K. J. (1994). New empirical relationships among magnitude, rupture length, rupture width, rupture area, and surface displacement. *Bulletin of the Seismological Society of America*, *84*(4), 974-1002.

Hanks, T.C., & Kanamori, H. (1979). A moment magnitude scale. *Journal of Geophysical Research, 84*(B5), 2348–2350. https://doi.org/10.1029/JB084iB05p02348

Dengler, L.A., Uslu, B., Barberopoulou, A., Borrero, J.C., Synolakis, C., 2008, The vulnerability of Crescent City, California, to tsunamis generated by earthquakes in the Kuril Islands region of the northwestern Pacific, *Seismol. Res. Lett.*, 79 (5), 608 – 619. https://doi.org/10.1785/gssrl.79.5.608

Wilson, R.I., Admire, A.R, Borrero, J.C., Dengler, L.A., Legg, M.R., Lynett, P., McCrink, T.P., Miller, K.M., Ritchie, A., Sterling, K., Whitmore, P.M., 2013, Observations and impacts from the 2010 Chilean and 2011 Japanese tsunami in California (USA), *Pure Appl. Geophys*., 170, 1127 – 1147, https://doi.org/10.1007/s00024-012-0527-z.

Lynett, P., Borrero, J., Weiss, R., Son, S., Greer, D., Renteria, W., 2012, Observations and modeling of tsunami-induced currents in ports and harbors, *Earth Planet. Sci. Lett*., 327 – 328, 68 – 74. https://doi.org/10.1016/j.epsl.2012.02.002

Lynett, P., Borrero, J., Son, S., Wilson, R., Miller, K., 2014, Assessment of the tsunami-induced current hazard, *Geophys. Res. Lett,* 41, 2048 – 2055. https://doi.org/10.1002/2013GL058680